

# Data on $J/\Psi \rightarrow \gamma(K^\pm K_S^0 \pi^\mp)$ and $\gamma(\eta \pi^+ \pi^-)$

D.V. Bugg <sup>1</sup>,

Queen Mary, University of London, London E1 4NS, UK

## Abstract

Data on  $J/\Psi \rightarrow \gamma(\eta \pi^+ \pi^-)$  and  $\gamma(K^\pm K_S^0 \pi^\mp)$  from 58M  $J/\Psi$  hadronic interactions in the BES II detector are analysed. They throw new light on  $J^P = 0^-$  mesons throughout the mass range up to 2 GeV, notably  $\eta(1440)$ . For the first time, this state is fitted including the full  $s$ -dependence of decays to  $a_0(980)\pi$ ,  $\eta\sigma$ ,  $K\bar{K}^*$ ,  $\kappa\bar{K}$  and  $f_0(980)\eta$ , including the dispersive term associated with this  $s$ -dependence. Two types of fit are reported. The first uses a single  $\eta(1440)$ . The second uses separate  $\eta(1405)$  and  $\eta(1475)$ . The strong  $s$ -dependence of P-wave production of  $K^*K$  shifts the fitted mass of  $\eta(1475)$  down to 1440 MeV. As a result, the two types of fit give almost identical results and the conclusion from these data is that there is no significant evidence for two separate resonances. In  $K\bar{K}\pi$ , there are definite though small contributions from  $f_1(1420)$  and  $f_1(1285)$ . The optimum fit requires either a small additional  $f_1(1510)$  or alternatively a small perturbation to the high mass tail of  $f_1(1420)$ . At higher masses, there is a broad  $J^P = 0^-$  peak in  $\eta\pi\pi$  at 1850 MeV. There is also a weak but definite signal consistent with  $\eta_2(1870) \rightarrow \eta\pi\pi$ .

PACS: 13.25.-k, 14.40.Cs

## 1 Introduction

The analysis reported here was done in the years 2002–3 in collaboration with two senior members of the BES collaboration. The work was funded by the Royal Society and Queen Mary College via an official agreement with the Chinese Academy of Sciences and the BES collaboration. This agreement guaranteed access to BES 2 data for the purpose of publications. Since then, the BES management has refused to appoint internal referees, hence blocking a collaboration publication and comments from the collaboration. The data illuminate the spectroscopy of  $J^P = 0^-$  mesons and should be in the public domain. There is a responsibility to publish work which has been supported from public funds with approximately £60,000. The wording of the article is close to a document submitted late in 2008 to the BES management, except for some clarification of wording.

There have been many earlier studies of  $\eta(1440)$  in  $J/\Psi$  radiative decays,  $\bar{p}p$  annihilation and  $\pi N$  interactions. Extensive references are to be found in the listings of the Particle Data Group (PDG) [1]. Their review concludes that two nearby  $0^{-+}$  resonances are required in the mass range 1400–1500 MeV. The lower one is at 1405 MeV, decaying to  $\eta\pi\pi$  and  $\kappa\bar{K}$ , where  $\kappa$  stands for the  $K\pi$  S-wave. The upper state is at 1475 MeV, decaying dominantly to  $K^*(890)\bar{K}$ .

However, almost all of these analyses are based on fitting the strong  $K^*(890)\bar{K}$  channel with a Breit-Wigner resonance of constant width. The threshold for this channel is at 1390 MeV, although smeared out to some extent by the 50 MeV full-width of the  $K^*$ . The  $K^*\bar{K}$  channel with  $J^P = 0^-$  is produced in a P wave. As a result, the intensity of the  $K^*\bar{K}$  channel

---

<sup>1</sup>email address: david.bugg@stfc.ac.uk

increases with kaon momentum  $k$  as  $k^3$ . This rapid  $s$ -dependence enhances the upper side of the  $K^*\bar{K}$  peak strongly. It also gives rise to a strong dispersive correction in the Breit-Wigner denominator, as described in subsection 4.3. Only one previous analysis includes the first feature and none contains the second. They are therefore prejudiced towards two separate resonances.

As well as the possible  $\eta(1405)$  and  $\eta(1475)$ , there is evidence from four experiments on  $\pi p \rightarrow (\eta\pi\pi)p$  for  $\eta(1295)$  [2], [3], [4] and [5]. In these data, the possible exchange of both natural and unnatural parity mesons requires a rank 2 analysis, with partial interference between the two alternatives, hence incomplete interferences between  $f_1(1285)$  and  $\eta(1295)$ . The possibility of no interference between  $f_1(1285)$  and  $\eta(1295)$  leaves some room for uncertainty in conclusions. There is no definite evidence for  $\eta(1295)$  in  $J/\Psi$  decays and only weak evidence in  $\bar{p}p$  annihilation [6].

There are therefore three controversial candidates for two radial excitations of  $\eta$  and  $\eta'$ . Some people have argued that  $\eta(1295)$  has been confused with  $f_1(1285)$  [7]. Others argue from the strong production of  $\eta(1405)$  and  $\eta(1475)$  in  $J/\Psi$  radiative decays that one of them is the  $0^-$  glueball [8]. However, Lattice Gauge calculations predict the glueball above 2 GeV [9].

One must remember too that the  $\eta$  and  $\eta'$  are well established to have compositions

$$\eta = n\bar{n} \cos \phi - s\bar{s} \sin \phi \quad (1)$$

$$\eta' = n\bar{n} \sin \phi + s\bar{s} \cos \phi, \quad (2)$$

where  $n\bar{n} = (u\bar{u} + d\bar{d})/\sqrt{2}$  and  $\phi = 41.5^\circ$  if there is no glueball component [10]. In  $J/\Psi$  radiative decays, the  $\eta'$  is produced with an intensity a factor 5 larger than the  $\eta$ . Similar mixing for radial excitations could explain surprisingly strong production of  $\eta(1405)$  and/or  $\eta(1475)$  in  $J/\Psi$  decays and  $\bar{p}p$  annihilation.

There are two likely scenarios. The first is that the  $\eta(1295)$  does not exist and  $\eta(1405)$  may be assigned dominantly as  $\bar{n}n$  and  $\eta(1475)$  as  $\bar{s}s$ . The second scenario is that  $\eta(1295)$  does exist and  $\eta(1405)$  and  $\eta(1475)$  are really one resonance. These two alternatives are fitted to data presented here. The  $s$ -dependence of the Breit-Wigner amplitudes is treated fully for the first time.

The higher mass range for  $\eta\pi\pi$  is also of considerable interest. BES II data provide evidence for a 7 standard deviation signal in  $\eta'\pi\pi$  for a narrow  $X(1835)$  with  $\Gamma = 68$  MeV [11]. It is important to know if it appears in  $\eta\pi\pi$  and if so with what branching fraction.

Section 2 presents technical details of the selection of data for the channels  $\gamma(\eta\pi^+\pi^-)$ ,  $\gamma(\eta K^+K^-)$  and  $\gamma(K^\pm K_S^0 \pi^\mp)$  and discusses backgrounds. The  $\gamma(\eta K^+K^-)$  channel has not been examined before. It is useful in establishing the magnitude of possible  $f_0(980)$  contributions to  $\eta K\bar{K}$ . Sections 3 and 4 present features of the data and the formulae needed to treat the  $s$ -dependence of Breit-Wigner amplitudes. Section 5 gives details of the fit to the mass range up to 1600 MeV. This is the centre-piece of the paper. Section 6 considers the high mass range above 1600 MeV and estimates the magnitude possible for  $X(1835) \rightarrow \eta\pi\pi$ ; the low value observed is inconsistent with the  $X(1835)$  being dominantly  $\bar{n}n$ . Section 7 returns to the interpretation of  $\eta(1440)$  and  $f_1(1510)$ . Section 8 summarises conclusions.

## 2 Data selection

The data fitted here were taken with the BESII detector. Full details of the detector and its upgrade are reported by Bai et al. [12], [13]. It has cylindrical symmetry around the intersecting  $e^+e^-$  beams. Its essential features are (i) a Main Drift Chamber (MDC) for the measurement of charged particles, (ii) time of flight detectors with a  $\sigma$  of 180 ps, and (iii) a 12 radiation length Barrel Shower Counter comprised of gas proportional tubes interleaved with lead sheets. The MDC measures  $dE/dx$ . Together with the time of flight detectors, it separates  $\pi$  and  $K$  up to  $\sim 700$  MeV/c. Outside the  $\gamma$  detectors is a magnet providing a field of 0.4T. This magnet is instrumented with muon detectors, but for present work they serve simply to reject  $\mu^+\mu^-$  pairs. The Main Drift Chamber provides full coverage of charged particles for lab angles  $\theta$  with  $|\cos\theta| < 0.84$ .

### 2.1 Selection of $\gamma(\eta\pi^+\pi^-)$ and $\gamma(\eta K^+K^-)$

These events have been selected by demanding exactly three photons and two charged tracks with balancing charges. Both charged particles must be positively identified by time-of-flight and/or  $dE/dx$  as pions (for  $\eta\pi^+\pi^-$ ) or as kaons (for  $\eta K^+K^-$ ). The vertex must lie within a cylinder of 1.5 cm radius, 30 cm long, centred on the intersecting  $e^+e^-$  beams. Two photons must have an invariant mass within 70 MeV of the  $\eta$ . Events are rejected if any two photons produce a mass within 40 MeV of the  $\pi^0$ . Photons may also originate from interaction of charged tracks in the detector. Any photons lying within a  $6^\circ$  cone around a charged track are discarded.

Candidate events have been subjected to 4-constraint kinematic fits to  $3\gamma\pi^+\pi^-$  and 5C fits to  $\gamma\eta\pi^+\pi^-$  (or correspondingly  $3\gamma K^+K^-$  and  $\gamma\eta K^+K^-$ ); they are accepted only if the  $\chi^2$  probability of each fit is  $> 5\%$ . Any events where two photons are consistent with the final state  $2\gamma\eta\pi^+\pi^-$  or  $2\gamma\eta K^+K^-$  are rejected if  $\chi^2 < 20$ . They are also rejected if the measured particles are consistent with the loss of one photon and a fit to  $4\gamma\pi^+\pi^-$  or  $4\gamma K^+K^-$  with  $\chi^2 < 20$ .

The main background arises from the loss of one photon from the final state  $\eta\pi^+\pi^-\pi^0$ , which is dominated by  $a_2(1320)\rho$ . This background has been studied using the standard SIMBES Monte Carlo simulation of the detector. After the loss of one soft photon, it leads to a strong peak at high  $\eta\pi\pi$  masses 2300-2800 MeV. This background may be reconstructed from data by assuming one missing photon in the kinematic fit. For events fitted this way, Fig. 1(a) displays the  $\pi^0\pi^\pm$  mass distribution. There is a clear peak due to  $\rho(770)$ . If  $M(\pi^0\pi^\pm)$  lies in the mass range 670–870 MeV, one finds the  $\eta\pi^\mp$  mass distribution of Fig. 1(b). It shows clear  $a_0(980)$  and  $a_2(1320)$  peaks. In order to suppress these backgrounds further, the missing momentum is calculated from the measured  $\eta\pi^+\pi^-$  of each candidate event. Assuming the missing particle to be a  $\pi^0$ , any event with  $M(\pi^0\pi^\pm)$  in the mass range 670-870 MeV is rejected. However, a minor problem is that events lying in the charge zero peak of the  $\rho$  cannot be eliminated without rejecting required  $\gamma\eta\sigma$  events, where  $\sigma$  is a shorthand for the  $\pi\pi$  S-wave.

Fig. 1(c) shows the mass distribution for the  $\gamma\gamma$  pair closest to the  $\eta$  for all combinations fitting  $3\gamma\pi^+\pi^-$ . Fig. 1(e) shows the corresponding plot for candidate  $\eta K^+K^-$  events. Fig. 1(d) shows the  $\eta\pi\pi$  mass distribution from the final data sample. Peaks are visible at 1285 and 1415 MeV, followed by a sharp rise at 1490 MeV to a shoulder at  $\sim 1550$  MeV. There is a further peak at  $\sim 1850$  MeV, then a rapid fall to 2 GeV.

Above 2 GeV, there is a large contamination from the background explained above. The

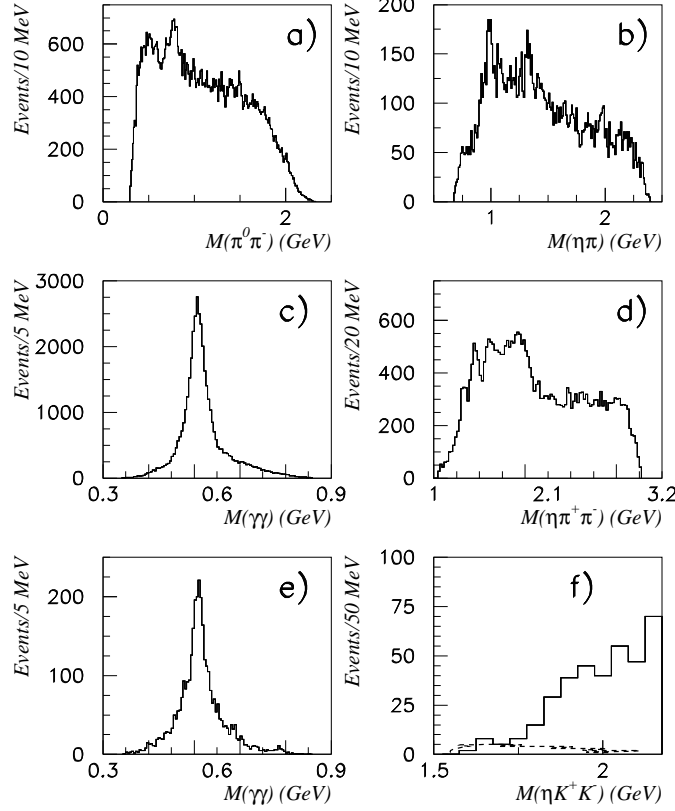


Figure 1: Mass distributions for (a)  $\pi^0\pi^\pm$  and (b)  $\eta\pi^\mp$  for events fitted to  $\pi^0\eta\pi^+\pi^-$  after selecting events with  $M(\pi^0\pi^\pm)$  in the range 0.67 to 0.87 GeV; (c) mass distributions for the  $\gamma\gamma$  pair closest to the  $\eta$  for  $3\gamma\pi^+\pi^-$  and (e)  $3\gamma K^+K^-$ ; (d)  $M(\eta\pi^+\pi^-)$  after a kinematic fit to  $\gamma\eta\pi^+\pi^-$ ; (f)  $M(\eta K^+K^-)$  after a kinematic fit to  $\gamma\eta K^+K^-$ ; the dashed curve shows the predicted mass distribution for  $f_0(980) \rightarrow K^+K^-$  from  $\eta(1440)$ .

Monte Carlo simulation of the  $a_2\rho$  background is fitted to events in the mass region 2300-2800 MeV, hence establishing its magnitude. It agrees with the PDG branching fraction of  $J/\Psi \rightarrow a_2(1320)\rho$  within its quoted error of 35%.

The physics analysis will be restricted to the mass range below 2 GeV. Since  $a_2(1320)\rho$  is the dominant background by a factor 10, the background at low  $\eta\pi^+\pi^-$  masses is taken from the Monte Carlo simulation of this channel. Integrated up to an  $\eta\pi\pi$  mass of 2 GeV, this background is 18.2%. Its distribution with  $\eta\pi\pi$  mass is illustrated below in Fig. 7(d). In the mass range below 1600 MeV it is small and featureless. Although there is a background of misidentified events, direct feedthrough from  $a_2\rho$  produces at most 33 events in  $\rho \rightarrow \pi^+\pi^-$ , mostly above 1600 MeV. This small  $a_2(1320)$  background surviving in data will be pointed out later.

At the end of the data selection, there are 18,751 events up to an  $\eta\pi\pi$  mass of 2000 MeV of which an estimated 3350 are background. The average efficiency for data reconstruction is 13.5%. The branching fraction is

$$BR[J/\Psi \rightarrow \gamma(\eta\pi\pi)] = (7.5 \pm 0.8(syst)) \times 10^{-3} \quad (3)$$

up to a mass of 2 GeV, after correction for all charge combinations and background. The error is mostly systematic. It covers the estimated background and the uncertainty in partial wave amplitudes due to loss of events through the  $35^\circ$  holes in the detector around the beam entrance and exit. The PDG quotes an average branching fraction  $(6.1 \pm 1.0) \times 10^{-3}$ . However, this refers to a Crystal Ball measurement [14] claiming a peak in  $\eta\pi\pi$  at 1700 MeV, substantially different to what is observed here.

## 2.2 Data on $J/\Psi \rightarrow \gamma(\eta K^+ K^-)$

For this final state, the main background arises from  $\pi^0\eta K^+ K^-$  after the loss of one photon. The contamination is estimated to be  $\sim 27\%$  from a study of side-bins either side of the  $\eta$  peak, together with a Monte Carlo estimate of the shape of the background. The reconstruction efficiency is 7.6% and varies little with  $\eta K \bar{K}$  mass. Fig. 1(f) shows the mass distribution of events fitting as  $\gamma\eta K^+ K^-$ . The number of events is too small to allow a meaningful physics analysis. However, the data are useful in establishing an upper limit on the number of events due to the final state  $f_0(980)\eta$ ,  $f_0 \rightarrow K^+ K^-$ . The essential point is that the number of signal events is a factor 100 smaller than for  $\gamma\eta\pi^+\pi^-$ . After background subtraction, there are 22 events up to an  $\eta K \bar{K}$  mass of 1.8 GeV and 125 up to 2 GeV. The latter corresponds to a branching fraction

$$BR[J/\Psi \rightarrow \gamma\eta K \bar{K}] = (1.4 \pm 0.4) \times 10^{-4} \quad (4)$$

up to 2 GeV. Errors are again systematic, from the acceptance.

## 2.3 Selection of $\gamma(K^\pm K_S^0 \pi^\mp)$ events

These events have been selected initially with at least one photon and with 4 charged tracks having balancing charges. One and only one charged kaon must be identified by time-of-flight or  $dE/dx$ ; at least two charged tracks must be positively identified as pions.

Events are then subjected to a  $4C$  kinematic fit, requiring a  $\chi^2$  probability  $> 5\%$ . The mass of one  $\pi^+\pi^-$  pair must lie within 25 MeV of the  $K_S^0$ . This pair must be consistent with a vertex within 6 cm of the second vertex defined by the other two charged particles. Fig. 2 shows the mass distribution for the reconstructed  $K_S^0$  before the kinematic fit. There is a clean peak with only a 4% background, which can be evaluated accurately. Events are rejected if the spectator pion and either of the other two particles (fitted as pions) have an invariant mass within 25 MeV of the  $K_S^0$ .

Events are rejected if there is a better fit to final states  $K^\pm K_S^0 \pi^\mp$  or  $K^\pm K_S^0 \pi^\mp \pi^0$  without an additional photon. In order to reject the second process more strongly, events are discarded if the missing mass attributed to neutral particles is within 50 MeV of the  $\pi^0$  mass.

The kinematic fit is made assuming that the  $K_S^0$  decays at the primary vertex; the effect of this assumption on the selection of events is simulated by a Monte Carlo study. There is a small loss of events, but no significant bias to kinematics. Alternative selections have been made fitting two separate vertices. These lead to a larger loss of events because of the difficulties of reconciling two vertices with the kinematics; within statistics, there is no change to physics conclusions.

At the end of the data selection, there are 5638 events including an estimated background of 1068. The background is substantially smaller over the reduced mass range up to 1600 MeV.

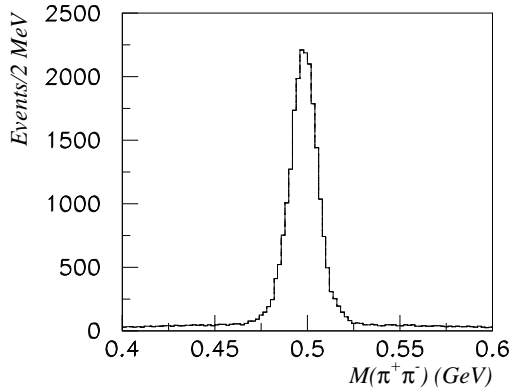


Figure 2: The mass distribution for the reconstructed  $K_S^0$ .

The average efficiency for data reconstruction is 10.8%. The resulting branching ratio, corrected for charge combinations, is

$$BR[J/\Psi \rightarrow \gamma K \bar{K} \pi] = [2.2 \pm 0.3(syst)] \times 10^{-3}, \quad (5)$$

up to a mass of 1800 MeV. The error is almost entirely systematic. A 10.3% error arises from extrapolating the partial wave analysis over the holes of the detector, 7.5% uncertainty in the effects of cuts, and 4.5% in the background; these errors are added in quadrature. The PDG quotes an average of  $(2.8 \pm 0.6) \times 10^{-3}$ , though this is derived from four values spanning the range  $(1.66 - 4.3) \times 10^{-3}$ .

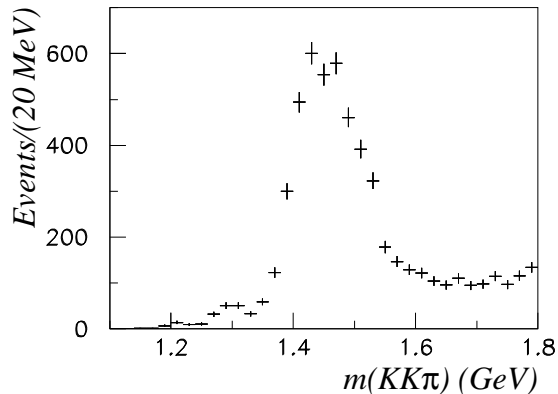


Figure 3: The  $K^\pm K_S^0 K^\mp$  mass spectrum.

The Monte Carlo used here to simulate the BES detector was the standard SIMBES package released in February 2002, in its version as of March 2003. During discussions with the BES management, they have claimed that alterations to the calibration of the time-of-flight system after March 2003 could affect the selection of events. This point is discussed in detail in the accompanying paper on  $\gamma(\pi^+\pi^-\pi^+\pi^-)$  data [15]. In that analysis, no systematic discrepancy is observed between  $(dE/dx)$  and time-of-flight, and the same is true for present data; no

contamination of  $\gamma\pi^+\pi^-\pi^+\pi^0$  events by  $\gamma K^+K^-\pi^+\pi^-$  is observed above the 1% level. In the present data, there is again no observed confusion between  $\pi^+\pi^-$  and  $K^+K^-$ . For  $\gamma\eta\pi^+\pi^-$  data, contamination from  $\gamma\eta K^+K^-$  is obviously  $< 1\%$  because of the small observed branching fraction for that channel. There is no evidence for contamination from  $\pi^0\eta K^+K^-$ , which is kinematically well separated from  $\gamma\eta\pi^+\pi^-$ ; such contamination is estimated to be  $< 1\%$ . For  $\gamma(K^\pm K_S^0\pi^\mp)$  data, the selection of the  $K_S^0$  limits possible background to 4%. The observed background under the  $K_S^0$  is consistent with that originating from  $\pi^0 K^\pm K_S^0\pi^\mp$ ; it rises with  $K\bar{K}\pi$  mass as expected for that source.

### 3 Features of the data

Fig. 3 shows the  $K\bar{K}\pi$  mass distribution in  $J/\Psi \rightarrow \gamma(K^\pm K_S^0\pi^\mp)$ . A small  $f_1$  peak is visible at 1285 MeV. Then there is a strong but asymmetric peak at  $\sim 1450$  MeV on a slowly rising background. There may be a small structure causing a drop at 1530 MeV, though this could be a large statistical fluctuation. A similar shoulder is visible at 1510 MeV in Mark III data of Bai et al. [16]. Several alternative prescriptions for fitting this shoulder will be described.

The raw mass distribution for  $\eta\pi^+\pi^-$  is shown in Fig. 1(d) and fits to it will be shown in detail below in Figs. 7 and 11. There is a narrow peak at  $1415 \pm 10$  MeV with a full width of 60 MeV. There is also a sharp rise at 1500 MeV. It is vital to realise from the outset that these structures are superimposed on a large and broad  $0^-$  signal extending over the whole mass range from 1200 to 2000 MeV and interfering coherently, see Fig. 7(b) below. Without the inclusion of this broad component, fits fail completely to describe the  $\eta\pi\pi$  mass projection. In particular, the broad component plays a major role in fitting the shoulder at 1550 MeV.

The  $\gamma 4\pi$  data contain a similar broad peak at 1600 MeV in  $\rho\rho$  with  $J^P = 0^-$  [15]. It is natural that some  $\rho\rho$  pairs will de-excite to  $\eta\sigma$  or  $a_0(980)\pi$  with  $L = 1$  in the decay. It is also possible that the  $\rho\rho$  peak at 1600 MeV is resonant.

Dalitz plots for  $\eta\pi^+\pi^-$  are shown for three mass ranges in Fig. 4. The upper 3 panels are for data and the second three from the fit to  $\eta(1440)$  reported below. The lower set does not contain the statistical fluctuations of the upper set and the plotting procedure makes it appear that there are some differences between data and fit. However, a check on all bins shows no evidence for systematic discrepancies. The main feature in all three cases is a peak due to two crossing  $a_0(980)$  bands.

Dalitz plots for  $K\bar{K}\pi$  are shown in Fig 5 for three mass ranges. Here, the main feature is due to two crossing  $K^*(890)$  bands. There is a strong enhancement near the intersection of these bands in Figs. 5(a) and (b). It is much reduced in Fig. 5(c). This is due to the zero in the  $K\pi$  amplitude near the middle of the  $K^*$  band, arising from the angular dependence of the partial wave amplitude in the decay.

## 4 Partial wave analysis

### 4.1 Preliminaries

The aim of the analysis is to fit the data in terms of conventional resonances, plus the broad interfering  $J^P = 0^-$  component observed both here and in the  $\gamma(\pi^+\pi^-\pi^+\pi^-)$  data. It would be

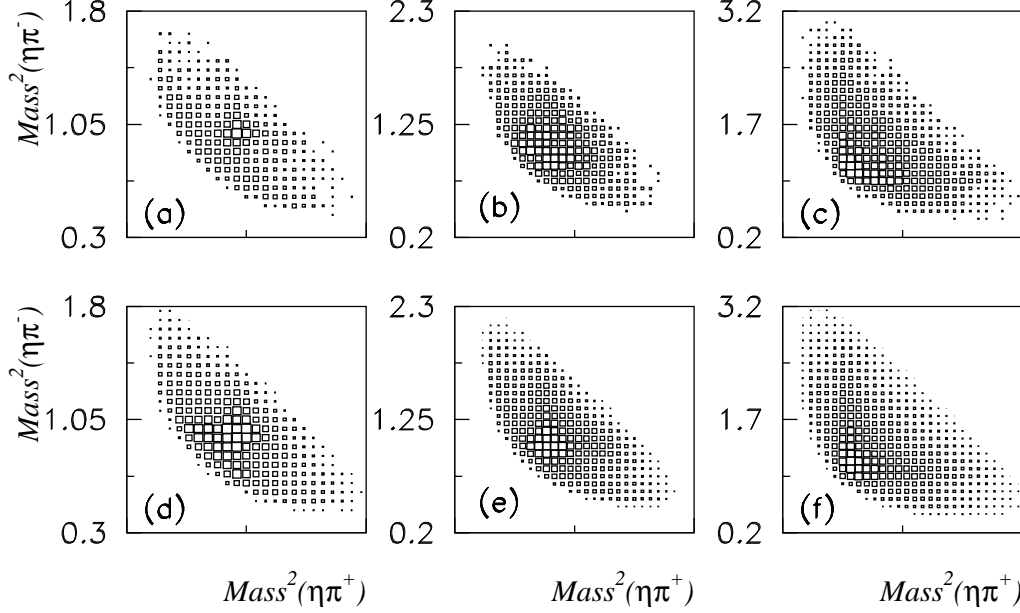


Figure 4: Dalitz plots for  $\eta\pi\pi$ : (a)–(c) show data and (d)–(f) the fit. Mass ranges for  $\eta\pi\pi$  are 1350–1480 MeV in (a) and (d), 1480–1620 MeV in (b) and (e), 1620–1950 MeV in (c) and (f).

good if the spin composition of  $\eta\pi\pi$  and  $K\bar{K}\pi$  could be determined in narrow slices of mass, and this has been tried. The main conclusion from that attempt is that  $0^-$  is strongly dominant for both sets of data. In  $K\bar{K}\pi$  data, contributions from  $J^P = 1^+$  are identified clearly in the narrow mass ranges of  $f_1(1285)$  and  $f_1(1420)$ . There is also definite evidence for a small  $1^+$  contribution continuing above  $f_1(1420)$ , up to  $\sim 1550$  MeV. However, it is sufficiently small that its line-shape cannot be determined with any precision from slice fits. The contribution from  $J^P = 2^-$  is small.

There are however two difficulties with trying to analyse the data in slices. The first is that the only available information is a differential cross-section. This does not allow independent determinations of amplitude and phase. A related difficulty is that there are complex interferences between  $a_0(980)\pi$ ,  $\eta\sigma$  and  $f_0(980)\eta$  in  $\eta\pi\pi$  data and likewise in  $K\bar{K}\pi$  data between  $K^*\bar{K}$ ,  $\kappa\bar{K}$  and  $a_0(980)\pi$ ,  $a_0(980) \rightarrow K\bar{K}$ . In the absence of any strong interferometer in the data with known quantum numbers, the slice analysis cannot sort out these interferences. This leaves no choice but to relate magnitudes and phases through Breit-Wigner amplitudes fitted directly to the data.

Partial waves which are tried are  $J^P = 0^-$ , (orbital angular momentum  $L' = 1$  in the production process  $J/\Psi \rightarrow \gamma + X$ ),  $1^+$  ( $L' = 0$ ),  $2^-$  ( $L' = 1$ ) and  $2^+$  ( $L' = 0$ ). Of these,  $J^P = 2^+$  is negligible. Decay channels which are considered are  $a_0(980)\pi$ ,  $K^*(890)\bar{K}$ ,  $\kappa\bar{K}$ ,  $a_2(1320)\pi$ ,  $f_2(1270)\eta$ ,  $f_0(980)\eta$  and  $\eta\sigma$ .

There is an immediate question how  $\sigma$  and  $\kappa$  should be parametrised. In  $\pi\pi$  and  $K\pi$  elastic scattering, there are Adler zeros which suppress the amplitudes strongly near threshold. This is well understood in terms of Chiral Symmetry Breaking, which creates the Adler zeros. However, in many sets of data, it is established that  $\sigma$  and  $\kappa$  appear as low mass peaks. The origin of this



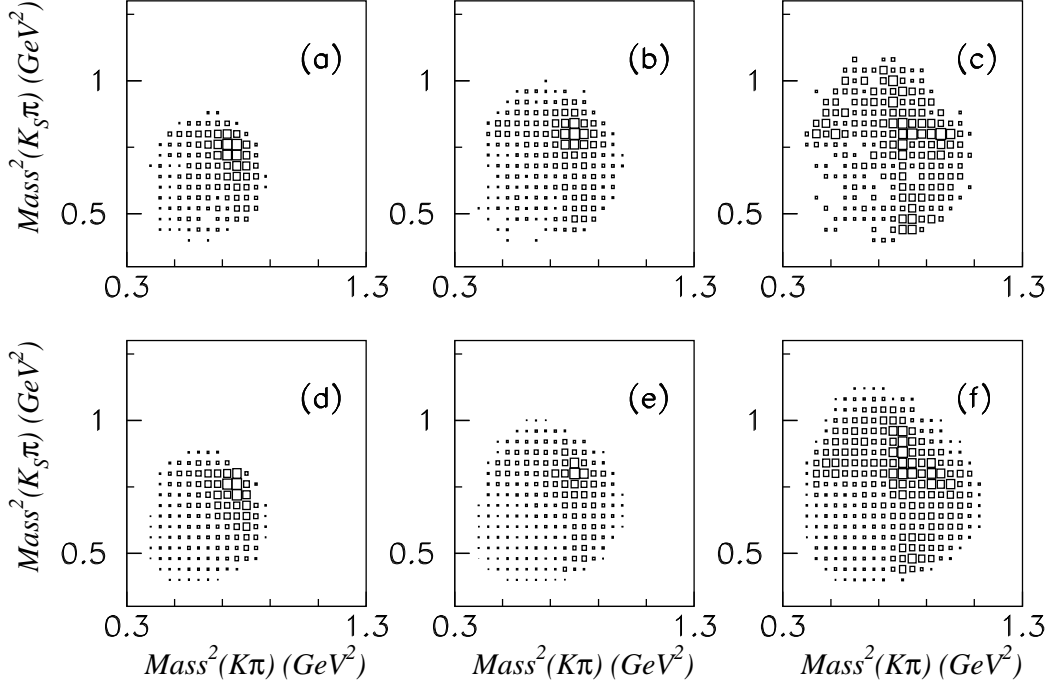


Figure 5: Dalitz plots for  $K^\pm K_S^0 \pi^\mp$ : (a)–(c) show data and (d)–(f) the fit. Mass ranges for  $K\bar{K}\pi$  are 1380–1440 MeV in (a) and (d), 1440–1500 MeV in (b) and (e), 1500–1560 MeV in (c) and (f).

effect is straightforward. If the elastic amplitude is written as  $N(s)/D(s)$ , the denominator must be universal. However, the numerator can be quite different in elastic scattering and production reactions. BES II data for  $J/\Psi \rightarrow \omega \pi^+ \pi^-$  [17] may be fitted accurately with  $N(s)$  a constant. This is also true for BES data on  $J/\Psi \rightarrow K \bar{K} \pi \pi$ , where there is again a low mass peak in the  $K\pi$  S-wave due to the  $\kappa$  pole [18]. The present work uses the  $\kappa$  amplitude fitted in Ref. [19] to LASS data for elastic scattering [20], BES II, and E791 data.

A problem is that it is not yet fully understood why or how the Adler zero disappears from the numerator of the amplitude in some production processes. In principle, there could be contributions with a numerator  $N(s) = A + Bs$  where  $A$  and  $B$  are complex constants. However, this unfortunately leads to large destructive interferences between the two terms. This is a well known symptom of over-fitting the data, so final fits must choose between  $\sigma$  and  $\kappa$  poles or alternatively amplitudes the same as for elastic scattering. Empirically, the present  $\gamma(K\bar{K}\pi)$  data give a considerably better fit (by 46 in log likelihood) with the  $\kappa$  pole amplitude, i.e. a constant numerator  $N(s)$ . [Log likelihood is defined here so that it changes by 0.5 for a one standard deviation change in the fit]. The  $\gamma(\eta\pi^+\pi^-)$  data show less discrimination, but still prefer a fit with the  $\sigma$  pole, i.e. no Adler zero in  $N(s)$ . This fit is better than one using the  $\pi\pi$  elastic scattering amplitude by 16 in log likelihood. Fits to present data are almost identical using the formula for the  $\sigma$  of Zou and Bugg [21] or a recent formula fitted to the  $\sigma$  pole [22]. The first formula is simpler and is used here. Both  $\sigma$  and  $\kappa$  are fitted using a constant for  $N(s)$ .

The fit to data is made using 200K Monte Carlo events for  $\gamma(\eta\pi^+\pi^-)$  and 52K for  $\gamma(K^\pm K_S^0 \pi^\mp)$

to simulate detector acceptance. These Monte Carlo events are generated with the standard SIMBES package. All figures show experimental results uncorrected for acceptance. These corrections are included automatically into the log likelihood fit. The acceptance varies only slowly across figures.

A technical detail is that partial wave amplitudes are written in terms of relativistic tensors; explicit formulae are given in [23]. In  $J/\Psi$  radiative decays, an important point is that the dominant production process is expected to be via intermediate  $\gamma c\bar{c}$ . Because of the high mass of these quarks and the interaction of the photon at a point, the production process is expected to be almost pointlike. Data on  $J/\Psi \rightarrow \gamma 4\pi$  in the accompanying paper verify this [15]. They contain a dominant  $J^P = 0^-$  signal in  $\rho\rho$  with a dependence on  $4\pi$  mass close to the expected  $P_\gamma^3$  for  $0^-$  production with  $L' = 1$ ; here  $P_\gamma$  is the photon lab momentum. The consequence for present data is that production should proceed only through the lowest available orbital angular momentum  $L'$ . There are well identified  $f_1(1285)$  and  $f_1(1420)$  signals in  $\gamma(K\bar{K}\pi)$  final states. In both cases, any amplitudes with  $L' = 2$  are negligible, producing improvements in log likelihood  $< 4$ . For production of  $0^-$  states, there is likewise no evidence for  $L' = 3$ . With this simplification, there are distinctive differences between final states with  $J^P = 0^-, 1^+, 2^-$  and  $2^+$ .

## 4.2 Details of partial wave fits

Fits to the 1450 MeV  $K\bar{K}\pi$  peak immediately reveal the need for both  $J^P = 1^+$  and  $0^-$  amplitudes. The  $f_1(1420)$  amplitude is conspicuous from its  $\cos\theta_d$  dependence, where  $\theta_d$  is the decay angle in the rest frame of the  $K^*$  to  $K$  and  $\pi$ . A free fit gives  $M = 1429 \pm 3$  MeV, compared with the value  $1426.4 \pm 0.9$  MeV of the PDG. If the  $f_1(1420)$  is removed from the final fit, log likelihood is worse by  $\geq 129$  for two less fitting parameters. Statistically this is nearly a 14 standard deviation effect.

There is also a small but definite  $f_1(1285)$  contribution, decaying to  $\kappa\bar{K}$ . If the  $\eta(1295)$  is included in the fit, its contribution is small and will be discussed in Section 7.

Earlier analyses have frequently fitted the  $a_0(980)$  freely to  $K\bar{K}\pi$  data. The  $a_0(980)$  contribution lies along the upper right-hand edge of Dalitz plots of Fig. 5. For low  $K\bar{K}\pi$  masses, it interferes strongly with the two  $K^*(890)\bar{K}$  components, see Figs. 5(a) and (b). It can easily be confused with the intersection between the two  $K^*(890)$  bands. The  $a_0(980)\pi$  contribution in  $\eta\pi\pi$  data does not suffer from this problem. Fits have therefore been made constraining the decay branching ratio of  $a_0(980)$  between  $\eta\pi$  and  $K\bar{K}$  to a value consistent with the Flatté form for  $a_0(980)$  [24]. Integrated over the  $a_0(980)$  peak up to 1.3 GeV, the branching fraction to  $K\bar{K}$  is  $(24 \pm 2)\%$  of that in  $\eta\pi$ . This constraint results in small but well defined contributions of  $a_0(980)$  to  $K\bar{K}\pi$  data. Production phases are fitted freely.

## 4.3 Parametrisation of amplitudes

It is essential to include into the Breit-Wigner amplitude the strong  $s$ -dependence of the phase space for P-wave production of  $K^*\bar{K}$ . This phase space rises as  $k^3$ , where  $k$  is the kaon momentum in the  $K^*K$  rest frame. As a reminder, the intensity for a two-channel resonance is

$$I(s) = \frac{M^2\Gamma_2(s)}{(M^2 - s)^2 + M^2\Gamma_{tot}^2(s)}, \quad (6)$$

where  $\Gamma_{tot}$  is the total width. The factor  $\Gamma_2(s)$  in the numerator arises from the phase space of the final  $K^*K$  state. The same  $s$ -dependence *must* be included into the denominator, otherwise an inconsistency with unitarity arises between numerator and denominator. The correct form for the Breit-Wigner amplitude for decay to channel  $j$  (for example  $K^*\bar{K}$ ) is

$$f_j = \frac{F_j B_j \rho_j(s)}{M^2 - s - m(s) - i \sum_i g_i^2 \rho_i(s) F_i^2 B_i^2}, \quad (7)$$

where  $g_i$  is the coupling constant for each channel  $i$  and  $\rho(s)$  is its phase space. A form factor  $F$  is included, and (where required) a centrifugal barrier factor  $B$ . Details will be given shortly. The evaluation of phase space is done numerically, using Eq. (40) of Ref. [25] which will be repeated here for completeness. As an example, the 3-body phase space for  $K^*\bar{K}$  is given by

$$\rho_{K^*\bar{K}}(s) = \int_{4m_K^2}^{(\sqrt{s}-m_K)^2} \frac{ds_1}{\pi} \frac{4|k||k_1|}{\sqrt{s s_1}} |T_{K^*\bar{K}}(s_1)|^2, \quad (8)$$

where  $T$  is the Breit-Wigner amplitude for the  $K^*$ . Here  $s$  refers to the resonance  $X$  and  $k$  to the momentum of the  $K^*$  or  $K$  in the rest frame of  $X$ ;  $s_1$  and  $k_1$  refer to the  $K^*$  and the momenta of decay  $K$  and  $\pi$  in its rest frame. For cases where there is angular momentum in the decay, the centrifugal barrier factor  $B$  appears in the numerator.

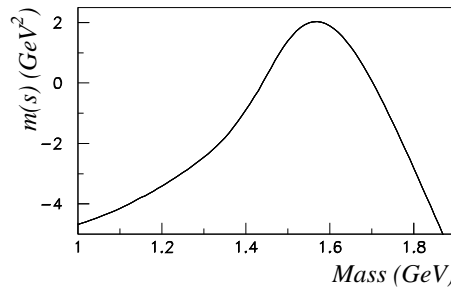


Figure 6: The dispersive term  $m(s)$  for  $\eta(1440)$ .

The term  $m(s)$  is a dispersive correction to the real part of the amplitude, required to make the amplitude fully analytic:

$$m(s) = \frac{M^2 - s}{\pi} \int \frac{M \Gamma_{tot}(s') ds'}{(s' - s)(M^2 - s')}. \quad (9)$$

It includes a subtraction on resonance making the integral strongly convergent. The resulting  $m(s)$  for  $\eta(1440)$  is illustrated in Fig. 6. In the 1440 MeV mass region, the term  $m(s)$  actually varies more strongly with  $s$  than the term  $(M^2 - s)$  in the Breit-Wigner denominator, leading to major deviations of phases from those of a Breit-Wigner resonance of constant width. This is one of the essential new features of the present analysis.

In fitting  $\eta\pi\pi$  data, it is unavoidable to introduce a broad  $J^P = 0^-$  signal. It needs to accomodate peaks observed in  $J/\Psi \rightarrow \rho\rho$ ,  $\omega\omega$ ,  $K^*\bar{K}^*$  and  $\phi\phi$  near their thresholds. A natural

explanation is that it arises from  $J/\Psi \rightarrow \gamma GG$ , where  $G$  are gluons, followed by coupling of gluons to vector mesons by colour neutralisation. An essential feature of the  $\gamma(\eta\pi\pi)$  data is the requirement for a peak at  $\sim 1600$  MeV, naturally associated with  $[\rho\rho]_{L=1} \rightarrow [\eta\sigma]_{L=1}$  and  $[a_0(980)\pi]_{L=1}$ . The strategy adopted here is to examine how far one can get by fitting this broad component by a single broad resonance  $X$  in the production process; exactly the same formula as (7) is used to fit  $\gamma(4\pi)$  data in the accompanying paper [15]. The mass  $M$  optimises empirically at  $(2.04 \pm 0.10)$  GeV. This is far removed from  $\eta(1440)$  so the only significant phase variation arises from (important) dispersive effects associated with the opening of each threshold. This broad background will be described as ‘the broad  $0^-$ ’.

Although Eq. (7) may look complicated, it is straightforward to programme and gives an excellent fit to present data and simultaneously to data on  $J/\Psi \rightarrow \gamma 4\pi$ . Each of the channels  $\eta\sigma$ ,  $a_0(980)\pi$ ,  $f_0(980)\pi$ ,  $K^*\bar{K}$ ,  $\kappa\bar{K}$ ,  $\rho\rho$ ,  $\omega\omega$ ,  $K^*\bar{K}^*$  and  $\phi\phi$  requires just one parameter  $g^2$  constrained (iteratively) to reproduce observed branching fractions of these channels. This constrains the  $s$ -dependence of the broad  $0^-$  amplitude closely. The first five channels are essential to fit  $\eta\pi\pi$  and  $K\bar{K}\pi$  data. The inclusion of the  $K^*\bar{K}^*$  threshold examines whether or not the drop in the  $\eta\pi\pi$  data above 1850 MeV can be explained by the  $K^*\bar{K}^*$  threshold. The channels  $\omega\omega$  and  $\phi\phi$  have little effect but are included for completeness.

Further details concern the form factor  $F$  and centrifugal barriers  $B$  in Eq. (7). The form factor for  $J/\Psi \rightarrow X$ ,  $X \rightarrow j$  is the product of a weak form factor  $F_p$  for the first step and a factor  $F_d$  for decays of  $X$  through channel  $j$ . Both are taken as Gaussians:

$$F = \exp(-\alpha_p K^2) \exp(-\alpha_d k^2), \quad (10)$$

where  $K$  is the production momentum of  $X$  in the  $J/\Psi$  rest frame and  $k$  is the decay momentum in the rest frame of  $X$  (for example, the momentum of  $\eta$  in the channel  $\eta\sigma$ ). Values of  $\alpha_p$  and  $\alpha_d$  are taken from the work on  $J/\Psi \rightarrow \gamma 4\pi$ :  $\alpha_p = 0.06 \text{ GeV}^{-2}$  and  $\alpha_d = 2.25 \text{ GeV}^{-2}$ , corresponding to RMS radii  $R_p = 0.12 \text{ fm}$ ,  $R_d = 0.73 \text{ fm}$ . The production form factor is very weak and has little effect here, but is included for consistency with  $\gamma(4\pi)$  data.

The factor  $B$  is likewise the product of the  $L' = 1$  centrifugal barrier for  $J/\Psi \rightarrow \gamma X$  and (where necessary) a centrifugal barrier for the decay, for example an  $L = 1$  barrier for the decay of  $0^-$  to  $K^*\bar{K}$ . As a reminder, for  $L = 1$ ,

$$B = kR/\sqrt{1 + k^2 R^2}; \quad (11)$$

the same value of  $R$  is used in the centrifugal barrier as in the form factor, though this may be an approximation.

## 5 Fits to data up to 1600 MeV

Two types of fit will be discussed. The first (Fit A in tables) tries to fit both  $\eta\pi\pi$  and  $K\bar{K}\pi$  data with a single  $\eta(1440)$  resonance. The second (fit B) uses two separate resonances like  $\eta(1405)$  and  $\eta(1475)$ , though their masses and widths need re-optimising.

Fig. 7 shows details of the fit to  $\gamma(\eta\pi\pi)$  data with a single resonance which optimises at a mass of  $1439 \pm 5$  MeV. Panel (a) shows the overall fit to the mass distribution; the lower histogram shows the coherent sum of  $\eta(1440)$  and the broad  $0^-$ . Panel (b) shows the full  $0^-$

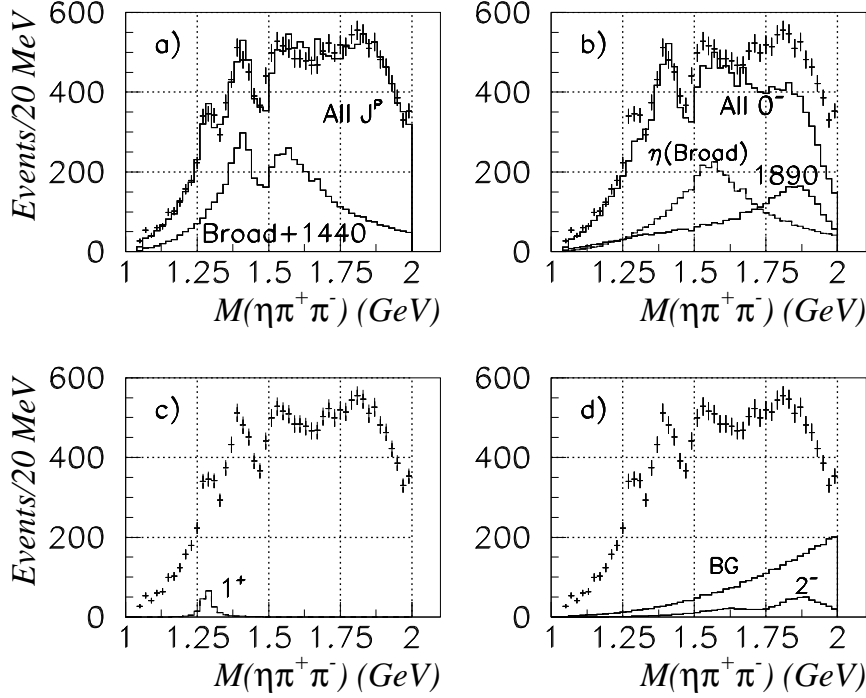


Figure 7: The fit to  $\eta\pi\pi$  data using  $\eta(1440)$ . Points with errors show data. In (a) the upper histogram shows the full fit; the lower one shows the coherent sum of  $\eta(1440)$  and the broad  $0^-$ ; (b) shows the total  $J^P = 0^-$  contribution; the lower histograms shows the broad  $0^-$  intensity from Eq. (7) and the  $\eta(1890)$  contribution; (c) the  $1^+$  intensity; (d) experimental background (BG) and the  $2^-$  contribution.

intensity, also the broad component from Eqs. (7)–(9) and thirdly  $\eta(1890)$ . Panel (c) shows the small peak due to  $f_1(1285)$ . Panel (d) shows background as the upper histogram and the small  $2^-$  contribution required above 1600 MeV from  $\eta(1645)$  and  $\eta(1870)$ . A detail is that it is necessary to check that the  $f_0(980)\eta$  contribution to  $\eta\pi\pi$  is consistent with data on  $\eta K^+ K^-$ . The dashed curve on Fig. 1(f) shows the signal predicted for  $f_0(980)\eta$  with  $f_0(980) \rightarrow K\bar{K}$ . It is consistent with data near 1600 MeV.

The sharp rise of the  $\eta\pi\pi$  mass distribution at 1495 MeV is not fitted perfectly in Fig. 7(a): the data would prefer a rise 10 MeV lower than the fit. The rapid rise requires a strong contribution from  $f_0(980)\eta$ . The fit which is shown uses the BES parametrisation of  $f_0(980)$  [26]. A reparametrisation is desirable including the threshold cusp in the real part of the amplitude at the  $K\bar{K}$  threshold. This has been tried, but does not cure the problem: it simply sharpens the  $f_0(980)$  peak near the  $K\bar{K}$  threshold.

Fig. 8 shows the fit to  $\gamma(K\bar{K}\pi)$  data. The peak sits on a small experimental background shown in (a) and a slowly rising physics background, clearly visible above experimental background. This physics background has  $J^P = 0^-$  and is parametrised by the broad  $0^-$  contribution decaying to  $K^*\bar{K}$ ,  $\kappa\bar{K}$  and  $a_0\pi$ ,  $a_0 \rightarrow K\bar{K}$ . The coupling constants of the first two are fitted freely; the last component is derived from the  $a_0(980)$  fitted to  $\eta\pi\pi$  data using the branching ratio between  $\eta\pi$  and  $K\bar{K}$  in Ref. [24].

The  $K\bar{K}\pi$  peak of Fig. 8 is decidedly asymmetric. The main source of the asymmetry can

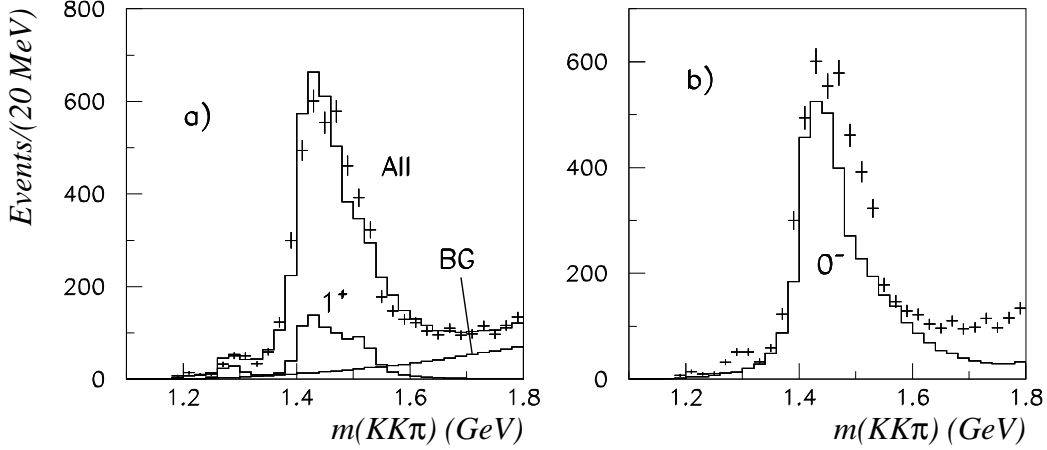


Figure 8: The fit to  $K\bar{K}\pi$  data. In (a) the upper histogram shows the full fit and the lower one the  $J^P = 1^+$  contribution from  $f_1(1285)$ ,  $f_1(1420)$  and  $f_1(1510)$ ; the experimental background is labelled BG. (b) shows the  $0^-$  contribution alone.

immediately be traced to the  $s$ -dependence of the  $K^*\bar{K}$  decay channel whose contribution is shown in Fig. 8(b). The lower histogram in Fig. 8(a) shows the contribution from  $J^P = 1^+$ . All fits require some  $1^+$  contribution above  $f_1(1420)$ ; this extra contribution is parametrised in the present fit by  $f_1(1510)$  with mass and width quoted by the PDG. Changing the parameters to values of Aston et al. [27] changes log likelihood only by 3.6.

Attempts have been made to fit the small shoulder in Fig. 8 at 1530 MeV in several ways. This mass is close to the opening of the  $K\bar{K}\eta$  channel at 1539 MeV. It raises the possibility of a drop in the line-shape associated with the opening of this channel; this is a unitarity effect - the opening of the  $\eta K\bar{K}$  channel robs  $K\bar{K}\pi$  of some signal. However, this is immediately excluded by the small branching ratio of  $\eta K\bar{K}$  compared to  $\eta\pi\pi$ . A more subtle possibility is that it may be associated with the  $f_0(980)\eta$  channel, which also peaks at 1539 MeV, since  $f_0(980)$  itself peaks at the  $K\bar{K}$  threshold. The fit to  $\eta\pi\pi$  data requires a strong contribution from  $f_0(980)\eta$ . However, it is spread out quite significantly according to phase space for the  $f_0(980)\eta$  final state, as shown below in Fig. 13(a); that is too broad to explain a narrow shoulder at 1530 MeV. Note that there is independent evidence for this  $f_0(980)\eta$  contribution to  $J^P = 0^-$  [28].

The  $f_2(1565) \rightarrow [a_2(1320)\pi]_{L=1}$  does not account for the 1550 MeV structure in  $\eta\pi\pi$  or the 1530 MeV shoulder in  $K\bar{K}\pi$ ; there is no visible  $a_2(1320)$  peak at this mass in  $\eta\pi$  or  $K\bar{K}$  and the angular dependence is wrong. Furthermore, the magnitude which can be fitted to  $f_2(1565)$  in  $\gamma 4\pi$  rules out the possibility of explaining the 1530 MeV shoulder with decays to  $[a_2(1320)\pi]_{L=1}$ .

One further possible explanation remains. In the accompanying paper on  $J/\Psi \rightarrow \gamma 4\pi$ , there is evidence that the  $\rho\rho$  peak at  $\sim 1600$  MeV is actually resonant at  $\sim 1560$  MeV. If this possible resonance has a weak decay to  $K^*\bar{K}$ , the shoulder at 1530 MeV can be fitted as an interference effect. The resulting fit is shown in Fig. 9 in identical format to Fig. 8; the addition of  $\eta(1560)$  with a width of 280 MeV improves log likelihood by 62. This explanation is clearly speculative. It is to be expected that two neighbouring resonances at 1440 and 1560 MeV will provide considerably more flexibility in the fit than  $\eta(1440)$  alone. However, the magnitude of the contribution from  $\eta(1560)$  is fairly small, as would be expected if its mixing with  $s\bar{s}$  is small;

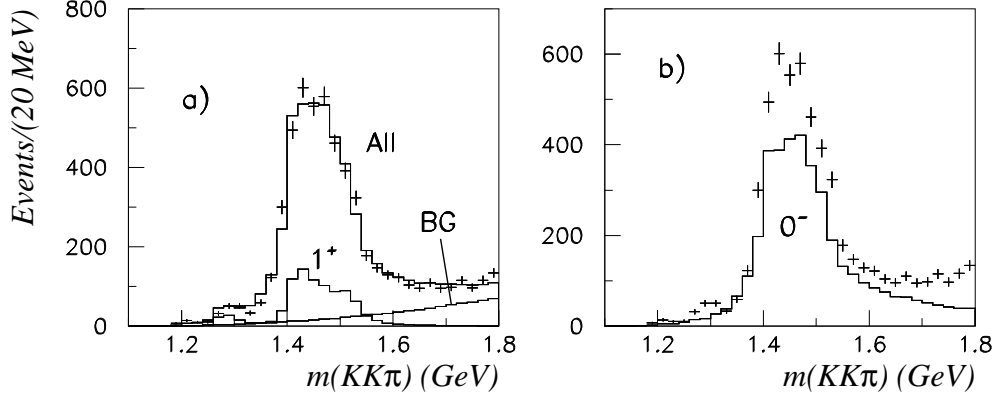


Figure 9: As Fig. 8 after the inclusion of  $\eta(1565)$ .

its intensity is 19% of that from  $\eta(1440)$ . This additional resonance does not provide the 10 MeV mass shift near 1500 MeV needed for a perfect fit to the  $\eta\pi\pi$  mass projection of Fig. 7(a). A possible remedy for this detail will be discussed in Section 7.

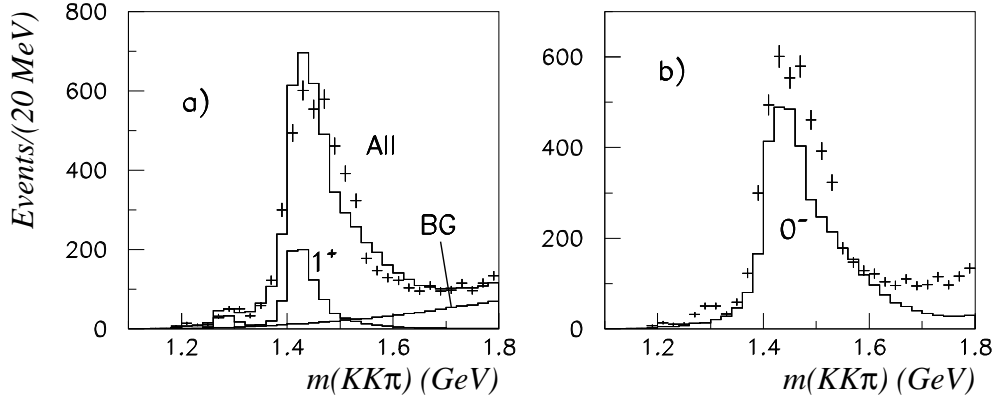


Figure 10: The fit to  $K\bar{K}\pi$  data without  $f_1(1510)$ . In (a) the upper histogram shows the full fit and the lower one the  $J^P = 1^+$  contribution from  $f_1(1285)$  and  $f_1(1420)$ ; (b) shows the  $0^-$  contribution alone.

Let us now turn to the  $J^P = 1^+$  contribution. Fig. 10(a) shows the poor fit without  $f_1(1510)$ . The remaining component due to  $f_1(1285)$  and  $f_1(1420)$  is shown as the lower histogram. The  $f_1(1420)$  is parametrised including the  $s$ -dependence of the  $K^*\bar{K}$  channel and the associated dispersive term. The result is to extend the tail of  $f_1(1420)$  to slightly higher masses, but does not substitute for  $f_1(1510)$ . The mass of  $f_1(1420)$  is held fixed at the PDG value and its full width at half maximum is fixed to the width quoted by the PDG. The magnitude fitted to  $f_1(1420)$  increases in Fig. 10 to 743 events compared with 488 in Fig. 8. The reason for this is the requirement for some significant  $1^+$  signal in the mass range around 1500 MeV. An alternative is to increase the width of  $f_1(1420)$  quite significantly. This possibility will be

discussed in Section 7.

## 5.1 The fit with separate $\eta(1405)$ and $\eta(1475)$

The full  $s$ -dependence is fitted to both states including the dispersive terms. This requires a determination of the channels which contribute to each.

The  $a_0(980)\pi$  and  $\eta\sigma$  channels are naturally attributed to  $\eta(1405)$ , as in earlier work. Attempts to include these channels into  $\eta(1475)$  lead to negligible contributions. The  $K^*\bar{K}$  channel is naturally associated with  $\eta(1475)$ , as in earlier work. If it is added to  $\eta(1405)$ , log likelihood improves only by 3.9, which is insignificant. Here, it is necessary to comment on earlier work of Adams et al. [5]. Their Fig. 4(d) shows a low mass  $K^*\bar{K}$  component in addition to that of  $\eta(1475)$ . However, from the present analysis it is clear that this is an artefact arising from their free fit to  $a_0(980)\pi$ ,  $a_0 \rightarrow K\bar{K}$ . The resulting large  $a_0(980)$  intensity in  $K\bar{K}\pi$  is inconsistent with the  $\eta\pi\pi$  data by a factor 10, so a constraint on the magnitude of  $a_0(980) \rightarrow K\bar{K}$  is essential. This eliminates any  $K^*\bar{K}$  contribution from  $\eta(1405)$ .

If  $\kappa\bar{K}$  is fitted freely to both  $\eta(1405)$  and  $\eta(1475)$ , it goes almost entirely into  $\eta(1405)$ . Removing the small component from  $\eta(1475)$  makes log likelihood worse by only 6.2, which is barely significant. Furthermore, it removes a destructive interference with  $K^*\bar{K}$ , symptomatic of instability. The final fit includes  $\kappa\bar{K}$  only in  $\eta(1405)$ .

The remaining component is  $f_0(980)\eta$ . It improves log likelihood of the fit by 162, a decisive amount. It plays a strong role in creating the sharp rise in the  $\eta\pi\pi$  mass projection of Fig. 7(a) at 1500 MeV. One might therefore naturally associate it with  $\eta(1475)$ . However, the fit contradicts this possibility. A free fit to both  $\eta(1405)$  and  $\eta(1475)$  leads to negligible contribution to  $\eta(1475)$  from  $f_0(980)\eta$ . It is easy to locate the reason. Associated with the  $f_0(980)\eta$  channel is a large dispersive term  $m(s)$  in the denominator of any resonance to which it couples. The phase variation created by this dispersive term is not compatible with  $\eta(1475) \rightarrow f_0(980)\eta$ . The final outcome is that  $\eta(1475)$  has only a  $K^*\bar{K}$  contribution and all other channels contribute via  $\eta(1405)$ .

The peak in  $\eta\pi\pi$  data is at  $1415 \pm 5$  MeV. However, because of the interference with the broad  $0^-$  contribution, the mass which can be fitted is quite flexible, with an uncertainty of  $\pm 20$  MeV. The fit actually optimises at 1429 MeV because the phase variation associated with  $m(s)$  in the Breit-Wigner denominator favours the higher mass.

For  $\eta(1475)$ , there is a strong correlation between the fitted width and the optimum mass. The strict optimum is at 1505 MeV. However, log likelihood is worse by only 4 if the PDG mass of 1476 MeV is used. In order to allow comparison with published results, the mass is fixed at the PDG average, 1476 MeV and the width is then optimised. The fitted width at half-maximum is 78 MeV, compared with the PDG average of  $85 \pm 9$  MeV. The fit to the  $\eta\pi\pi$  mass distribution using these values is shown in Fig. 11. Near the 1415 MeV peak, it is somewhat different in shape to that of Fig. 7. The fit to the rapid rise at 1500 MeV is no better than in Fig. 7(a).

The fit to  $K\bar{K}\pi$  data is shown in Fig. 12. The mass distribution of the peak is fitted rather better than in Fig. 8. The reason is obvious: two resonances allow much greater flexibility. In particular, the phase variation with  $s$  allowed by 2 resonances has much greater freedom than the fixed relation between magnitude and phase for  $\eta(1440)$  alone. With two resonances, it is possible to arrange that the mass distribution in Fig. 12 rises rapidly and falls rapidly, but with something approaching a flat top.



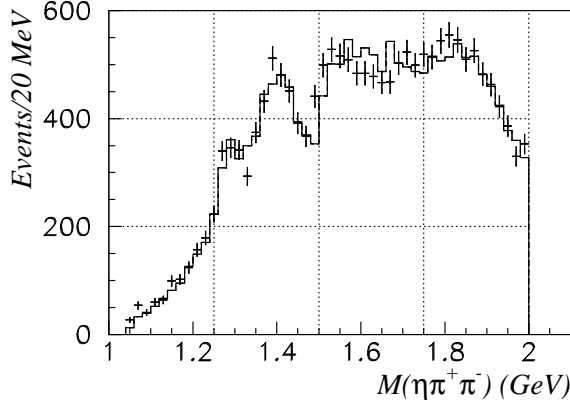


Figure 11: The fit to the  $\eta\pi\pi$  mass distribution using both  $\eta(1405)$  and  $\eta(1475)$ .

However, there is very little difference in log likelihood between fits with one resonance or two. The fit to  $\eta\pi\pi$  data with two states is better by 6.5 in log likelihood and the fit to  $K\bar{K}\pi$  data is better by only 2.6, making a total of 9.1 for the two sets of data. This hardly warrants confidence in the need for two resonances.

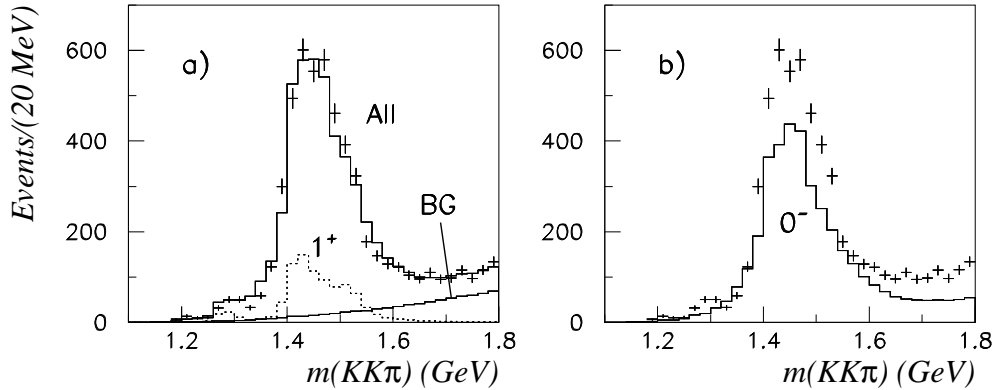


Figure 12: The fit to the  $K\bar{K}\pi$  mass distribution using both  $\eta(1405)$  and  $\eta(1475)$ .

Table 1 shows changes in log likelihood for both types of fit when individual components are removed and magnitudes and phases of all other components are re-optimised. The third column shows results for fit A with one resonance,  $\eta(1440)$ , and the fourth shows results for fit B with two resonances. This Table also includes branching fractions for channels or combinations of channels (where interferences are large). A warning is that for  $\eta(1440)$  there are strong interferences between  $\kappa\bar{K}$  and  $K^*\bar{K}$  and these are somewhat different for fits A and B. There are likewise large interferences between  $\kappa\bar{K}$  and  $K^*\bar{K}$  for the broad  $0^-$  signal. Errors given for branching fractions cover uncertainties in interferences. Because of large interferences between the broad  $0^-$  and  $\eta(1890)$ , branching fractions of Table 1 do not add up to the total branching fraction given in Eq. (5).

The one feature which might favour a fit with two resonances rather than one is the  $f_1(1510)$

contribution. Its parameters are fixed at PDG averages:  $M = 1518$  MeV,  $\Gamma = 73$  MeV. It improves the fit with a single  $\eta(1440)$  and an  $f_1(1510)$ , which is regarded by some authors as questionable, by 54.0. The improvement for the fit with 2 resonances is 38.9. So the fit without any  $f_1(1510)$  is better for fit B. Both fits require some  $f_1(1510)$  contribution, or something resembling it. A test has been made of the requirement for  $f_1(1510)$ , as distinct from a  $0^-$  contribution. A further  $0^-$  state is added to fit B using  $\eta(1405)$  and  $\eta(1475)$ . It is given identical mass and width to  $f_1(1510)$ . The result is that the  $f_1(1510)$  contribution dominates over that from  $\eta(1510)$ , confirming a definite requirement for a  $1^+$  component in this mass range. In Section 7, a possible explanation in terms of the line-shape of  $f_1(1420)$  will be presented.

Resonance	Channel	Fit A	Fit B	Br. Fr. (A)	Br. Fr. (B)
$\eta(1440)$ or $\eta(1405 + 1475)$	$a_0\pi, a_0 \rightarrow KK$	8.7	8.1	0.1	0.15
	$\kappa\bar{K}$	131	80	$2.1 \pm 0.3$	$3.3 \pm 0.5$
	$K^*\bar{K}$	441	382	$2.5 \pm 0.4$	$3.8 \pm 0.6$
	$a_0\pi, a_0 \rightarrow \eta\pi$	47	55	$0.40 \pm 0.15$	$0.6 \pm 0.2$
	$\eta\sigma$	39	81	$0.3 \pm 0.1$	$0.4 \pm 0.1$
	$f_0(980)\eta$	151	162	$1.0 \pm 0.3$	$1.5 \pm 0.6$
Broad $0^-$	$a_0\pi, a_0 \rightarrow KK$	10	10		
	$\kappa\bar{K}$	147	34	$1.6 \pm 0.7$	$1.3 \pm 0.4$
	$K^*\bar{K}$	132	111	$1.8 \pm 0.5$	$3.3 \pm 1.0$
	$a_0\pi, a_0 \rightarrow \eta\pi$	115	123		
	$\eta\sigma$	80	141		
	$\eta\sigma + a_0\pi \rightarrow \eta\pi\pi$			$18.4 \pm 9.7$	$19.0 \pm 10.0$
$\eta(1890)$	$a_0\pi, a_0 \rightarrow K\bar{K}$	16	21		
	$a_0\pi, a_0 \rightarrow \eta\pi$	177	197		
	$\eta\sigma$	134	157		
	$f_0(980)\eta$	81	107	$1.2 \pm 0.2$	$1.4 \pm 0.2$
	$\eta\sigma + a_0\pi \rightarrow \eta\pi\pi$			$15.3 \pm 9.7$	$16.4 \pm 10.0$
$f_1(1285)$	$\kappa\bar{K}$	70	143	$0.18 \pm 0.03$	$0.14 \pm 0.03$
	$a_0\pi, a_0 \rightarrow \eta\pi$	92	105	$0.9 \pm 0.3$	$0.9 \pm 0.3$
	$\eta\sigma$	9	11		
$f_1(1420)$	$K^*\bar{K}$	129	152	$0.6 \pm 0.1$	$1.3 \pm 0.2$
$f_1(1510)$	$K^*\bar{K}$	54	39	$0.4 \pm 0.1$	-
$\eta_2(1645)$	all $\eta\pi\pi$	11	11	$0.10 \pm 0.03$	$0.10 \pm 0.03$
$\eta_2(1870)$	all $\eta\pi\pi$	83	84	$1.1 \pm 0.3$	$1.1 \pm 0.3$

Table 1: Changes in log likelihood when individual components are removed and all other components are re-optimised in magnitude and phase. Column 3 shows results fitting  $\eta(1440)$  alone and column 4 results fitting both  $\eta(1405)$  and  $\eta(1475)$ . Columns 5 and 6 show branching fractions for  $J/\Psi \rightarrow \gamma + X$ , multiplied by  $10^4$ .

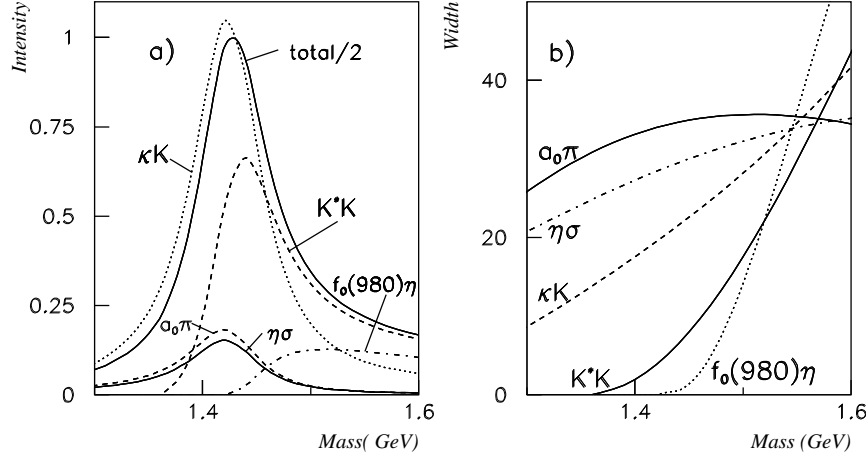


Figure 13: (a) Contributions to the line-shape of  $\eta(1440)$ , Fit A; (b) the variation with mass of phase space for each channel. The  $a_0\pi$  signal refers to  $\eta\pi\pi$ ; that for  $a_0 \rightarrow K\bar{K}$  is 24% of the signal in  $\eta\pi\pi$ .

## 5.2 Further details of the fit with $\eta(1440)$

Fig. 13(a) shows as the full curve the overall line-shape of  $\eta(1440)$ , scaled down by a factor 2 in order to display other contributions. The peak for  $K^*\bar{K}$  is at 1440 MeV, but there is a pronounced tail at high mass. One should note that in Obelix and Crystal Barrel data, this high mass tail is suppressed strongly by the phase space for production in  $\bar{p}p$  annihilation at rest.

From Fig. 13(a) it is quite difficult to decide on the centre of gravity of the  $K^*\bar{K}$  contribution. Averaging this contribution up to 1600 MeV it is at 1474 MeV, remarkably close to the PDG mass for  $\eta(1475)$ , namely 1476 MeV. Putting this in reverse, if one unfolds the expected  $s$ -dependence of  $K^*\bar{K}$ , the resonance mass should be expected at 1440 MeV, and agrees with the fit with a single resonance. The  $f_0(980)$  channel has a weak maximum near 1530 MeV, but also extends strongly to high mass. At high mass there are strong interferences between  $K^*\bar{K}$  and  $\kappa\bar{K}$ . Constructive interferences between them shifts the peak in  $K\bar{K}\pi$  up to 1450 MeV. Fig. 13(b) shows the dependence of phase space for each channel on mass, but with an arbitrary scale for each channel, so as to fit all the curves on to one figure.

Fig. 14(a) shows the Argand diagram for the coherent sum of  $a_0(980)\pi$  amplitudes from  $\eta(1440)$  and the broad  $0^-$  signal on which it sits. The diagram is drawn for an  $a_0(980)$  mass of 980 MeV, so as to avoid the effect of phase space on the integrated amplitude. Numbers on the figure indicate  $\eta\pi\pi$  masses in GeV. Fig. 14(b) shows the Argand diagram for the  $\eta\sigma$  amplitude evaluated for a  $\sigma$  mass of 800 MeV. Up to 1415 MeV, the real parts of the amplitudes are large. The dispersive contribution to the real part is large because the amplitude senses the steep rise at higher masses in the imaginary part - an impending barrier, which gets closer as the mass rises. As the  $K^*\bar{K}$  channel opens, there are two effects. Firstly, it increases the magnitude of the Breit-Wigner denominator and damps all  $\eta\pi\pi$  amplitudes. Secondly, the real part of the amplitude is approximately proportional to the gradient of the imaginary part. It turns over

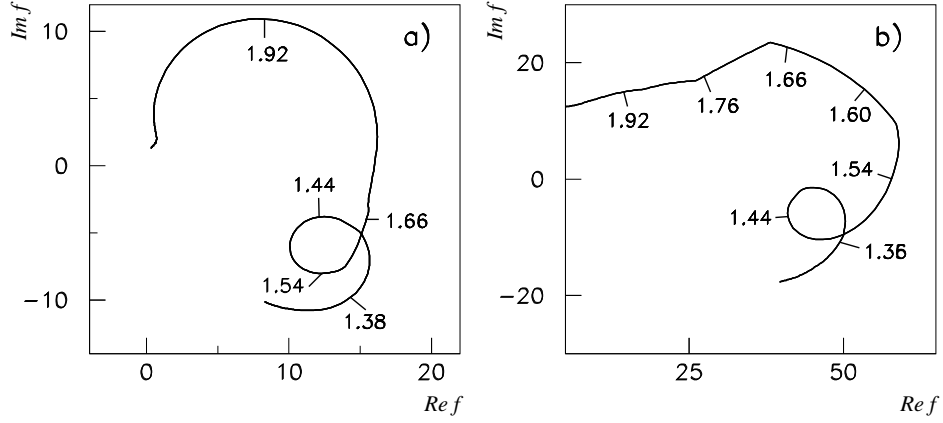


Figure 14: Argand diagrams for (a)  $a_0(980)\pi$  and (b)  $\eta\sigma$  for the coherent sum of  $\eta(1440)$  and the broad  $0^-$  contribution. Masses are marked in GeV.

rapidly at 1420 MeV and plunges through zero on resonance at 1440 MeV; these two features produce the narrow peak at 1415 MeV in  $\eta\pi\pi$ . The  $f_0(980)\pi$  amplitude contributes strongly to the steep rise in  $\eta\pi\pi$  at 1500 MeV. The cusp at 1600 MeV in the broad  $0^-$  contribution is largely responsible for the shoulder in  $\eta\pi\pi$  data at 1550 MeV.

Table 2 gives branching ratios integrated from threshold up to 1.8 GeV. Systematic errors from this cut-off are a factor  $(1.0 \pm 0.1)$  if the cut-off is reduced to 1650 MeV or increased to 2100 MeV. Errors cover variations observed in many alternative fits; they also cover the (small) discrepancies between the fits with one resonance or two. Note that there is large interference between  $a_0(980)\pi$  and  $\eta\sigma$ .

Channel	Branching fraction (%)
$K^*K$	$40 \pm 5$
$\kappa\bar{K}$	$35 \pm 5$
$\eta\sigma$	$4.1 \pm 1.6$
$a_0\pi, a_0 \rightarrow \eta\pi$	$5.5 \pm 2.1$
$a_0\pi, a_0 \rightarrow K\bar{K}$	$1.3 \pm 0.5$
$f_0(980)\eta$	$14 \pm 3$

Table 2: Branching fractions of  $\eta(1440)$ .

### 5.3 The branching ratio $K\bar{K}\pi/\eta\pi\pi$

From Table 2, the ratio

$$\frac{BR(\eta(1440) \rightarrow K\bar{K}\pi)}{BR(\eta(1440) \rightarrow \eta\pi\pi)} = 3.0^{+1.5}_{-0.9}. \quad (12)$$

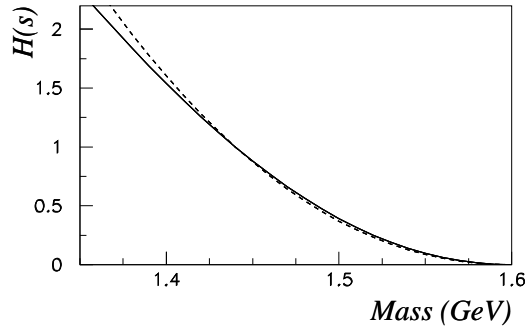


Figure 15: The factor  $H(m)$  allowing for the phase space and dynamics of the production process  $\bar{p}p \rightarrow \eta(1440)\sigma$  as a function of the mass  $m$  of  $\eta(1440)$ . The full curve shows production via the  $\sigma$  pole for the spectator pair and the dashed curve the result using the  $\pi\pi$  elastic scattering amplitude. It is normalised to 1 at 1440 MeV.

The errors have been obtained by adding in quadrature the errors for  $K^*\bar{K}$  and  $\kappa\pi$  to get overall branching fractions for  $K\bar{K}\pi$  in the range  $(82 - 68)\%$ , then dividing by the corresponding  $\eta\pi\pi$  fraction.

In their review, Masoni et al. [8] present in their Table 8 their estimate of the same branching ratio, or more exactly its inverse. Converting their entries to the definition used here, they estimate values in the range  $0.98 \pm 0.37$  from Mark III and DM2 data,  $0.30 \pm 0.1$  using Crystal Barrel and bubble chamber data of Baillon et al. [29], or  $0.11 \pm 0.05$  from Crystal Barrel and Obelix data. They use the disagreement between these sources as an argument in favour of separate  $\eta(1405)$  and  $\eta(1475)$ .

However, this analysis is misleading. When one analyses data for  $\bar{p}p$  annihilation, it is vital to allow for the suppression of the  $K^*\bar{K}$  channel by the available phase space. This was ignored by Masoni et al. The factor  $H(m)$  multiplying the line-shape of  $\eta(1440)$  is:

$$H(m) = \int_{4m_\pi^2}^{(2M_p - \sqrt{s_1})^2} ds_1 \frac{|p_{prodn}|}{2M_p} \frac{|p_1(\sigma \rightarrow \pi\pi)|}{\sqrt{s_1}} |T_\sigma(s_1)|^2 |F(p_{prodn})|^2. \quad (13)$$

Here  $s_1$  is the mass squared of the spectator  $\pi\pi$  pair, and  $p_{prodn}$  is the momentum of  $\eta(1440)$  or the spectator  $\sigma$  in the  $\bar{p}p$  rest frame. Next,  $M_p$  and  $m_\pi$  are the masses of the proton and pion. Also  $T_\sigma$  is the scattering amplitude for the spectator  $\pi\pi$  S-wave pair and  $F$  is the form factor for the production process, taken here as  $\exp(-2.25p_{prodn})$  with  $p_{prodn}$  in GeV/c.

The variation of  $H(m)$  with the mass of  $\eta(1440)$  is shown in Fig. 15. It is not clear whether the  $\pi\pi$  spectator pair will be produced via the  $\sigma$  pole or via the  $\pi\pi$  elastic scattering amplitude. The former is shown as the full curve and the latter as the dashed curve. They are sufficiently close that one can work with the average. The high mass tail of  $\eta(1440)$  is cut off strongly in  $\bar{p}p$  annihilation. It goes to zero at 1.60 GeV: the highest mass which can be produced in  $\bar{p}p$  annihilation with two spectator pions.

There are two consequences. Firstly, the factor  $H(m)$  amplifies the lower side of  $\eta(1440)$  with respect to the upper side. For the narrow  $\eta\sigma$  and  $a_0(980)$  channels, the effect is to shift the apparent peak of  $\eta(1440)$  downwards by 4.7 MeV; i.e. the Breit-Wigner mass is actually 4.7 MeV

higher than is fitted with a Breit-Wigner amplitude of constant width. For the  $\kappa K$  channel, the effect is larger because the phase space for this channel, shown on Fig. 13(b), increases significantly with  $m$ . The result is that the mass fitted to this channel is moved downwards by 9.7 MeV, so the true mass fitted as a Breit-Wigner resonance of constant width should be increased by this amount.

The second effect is that a considerable part of the  $K\bar{K}\pi$  signal is lost in data on  $\bar{p}p$  annihilation; all of it is lost above 1.60 GeV.

A check will be presented here on the ratio  $K\bar{K}\pi/\eta\pi\pi$  from data on  $\bar{p}p$  annihilation. Attention will be drawn to many sources of uncertainty. The check is done using data of Anisovich et al. [6] for  $\bar{p}p \rightarrow (\eta\pi^+\pi^-)(\pi^+\pi^-)$  and bubble chamber data of Baillon et al [29]. Table 2 of Anisovich et al. gives branching fractions for all amplitudes fitted to their data, in particular  $\eta(1440) \rightarrow \eta\sigma$  and  $a_0(980)\pi$ . This Table reveals an important point. There is large destructive interference in those data between these two amplitudes. This destructive interference has a strong effect on the branching fraction quoted for  $\eta(1440)$ . However, in reality there are major uncertainties in determining the interference. There are actually four charge combinations in those data allowing considerable freedom in interferences. The individual contribution from  $\eta\sigma$  is quoted as  $2.31 \times 10^{-3}$ , that from  $a_0(980)\pi$  is  $9.6 \times 10^{-3}$  and the interference between them contributes  $-2.28 \times 10^{-3}$ . It clearly makes a large difference how this interference is taken into account.

Relative magnitudes of all decay channels of a resonance should be the same in all production processes. The procedure adopted by Anisovich et al., and used here, is to derive coupling constants from the fit to data, then evaluate the intensity of amplitudes by taking the modulus squared of individual amplitudes. Interference between decay channels of one resonance are kept, since these are a property of the resonance. Interferences with other resonances in the data are ignored because such interferences are a feature of the particular environment in which the  $\eta(1440)$  is produced.

The resulting branching fraction for production of  $\eta(1440)$  in  $\eta\pi\pi$  via  $\bar{p}p$  annihilation is  $1.09 \times 10^{-3}$  in the observed charge states. This needs to be multiplied by a factor 9/4 to allow for other charge states, giving a result of  $2.45 \times 10^{-3}$  for  $\bar{p}p \rightarrow \eta(1440)$ ,  $\eta(1440) \rightarrow \eta\pi\pi$ . The result for all charges of  $K\bar{K}\pi$  quoted by Baillon et al. is  $(2.0 \pm 0.2) \times 10^{-3}$ . This gives a ratio  $R_{1440} = BR(\eta(1440) \rightarrow K\bar{K}\pi)/BR(\eta(1440) \rightarrow \eta\pi\pi) = 0.82$ . Masoni et al. use the smaller branching ratio  $0.61 \pm 0.19$  found by Amsler et al. [30] in an earlier analysis of  $\bar{p}p$  data. However, that publication does not specify if any allowance is made for the effect of destructive interference between  $\eta(1440) \rightarrow \eta\sigma$  and  $a_0(980)\pi$ .

The effect of  $H(m)$  on the integrated intensities for final states  $\eta\sigma$  and  $a_0(980)\pi$  is small because the phase space  $\rho(s)$  for these channels varies slowly with  $m$  and there is an approximate cancellation between upper and lower sides of the resonance. For the  $\kappa\bar{K}$  channel, there is a noticeable effect because of its fairly rapidly increasing phase space, see Fig. 13(b). Using Fig. 15, the  $\kappa\bar{K}$  component in  $\bar{p}p$  annihilation needs to be multiplied by a factor 1.38 and the  $K^*\bar{K}$  contribution needs to be multiplied by  $\sim 3.1$ . If we take the relative contributions of  $K^*\bar{K}$  and  $\kappa\bar{K}$  to be in the ratio 40:35 of Table 2, the result is to increase the  $K\bar{K}\pi$  branching fraction of Baillon et al by a factor 2.3, resulting in a value  $R_{1440}$  of 1.88.

This is still a little smaller than the value derived from Table 2, namely  $3.0^{+1.5}_{-0.9}$ . However, the essential conclusion is that the branching fraction between  $K\bar{K}\pi$  and  $\eta\pi\pi$  is subject to a large systematic correction when evaluated from  $\bar{p}p$  data. The result from  $J/\Psi$  data does not suffer

from these systematic problems. Note that the line-shapes fitted to present data are perturbed by the slowly varying factor  $P_\gamma^3$  for production with  $L' = 1$ ; this factor and the associated form factor have been included in the fit and the arithmetic of branching ratios. One should also note that the signal assigned by Obelix to the  $K\bar{K}\pi$  channel is not visible as a peak in the data, but is obtained from the difference in the line-shape of the  $K\bar{K}\pi$  signal from a Breit-Wigner of constant width fitted to  $\eta(1405)$ . A further detail is that the phases of individual decay channels are affected by multiple scattering with other components of the fit. They may differ from one production process to another. As a result, it is difficult to give a definitive result for the branching ratio between  $K\bar{K}\pi$  and  $\eta\pi\pi$ .

The reality of the situation is that there is major flexibility in the magnitudes of contribution which can be fitted to  $\eta(1440)$  in  $\eta\pi\pi$  channels. In the data presented here, there is flexibility in what can be fitted to the broad interfering component. This flexibility is apparent from the fact that fits with a single  $\eta(1440)$  or separate  $\eta(1410)$  and  $\eta(1475)$  differ very little in log likelihood. There is yet further flexibility if the  $\eta\sigma$  channel receives additional contributions proportional to the  $\pi\pi$  elastic amplitude.

## 6 Fits to data above 1600 MeV

In  $\eta\pi\pi$  data shown in Fig. 7, the broad  $0^-$  signal in Fig. 7(b) obviously fails to explain fully the  $\eta\pi\pi$  signal above 1600 MeV. The  $K^*\bar{K}^*$  threshold may contribute something to the drop above 1870 MeV, but alone does not fit the high mass spectrum. The remedy adopted here is to fit a resonance form as an expedient, although there is no phase information, hence no definite evidence for a resonance. The optimum fitted mass and width are  $1890 \pm 20$  MeV,  $\Gamma = 260 \pm 35$  MeV. The strongest decays are to  $a_0(980)\pi$ , but there is also a rather strong decay to  $f_0(980)\eta$ . Fig. 16 show mass projections from  $\eta\pi\pi$  Dalitz plots on to  $\pi\pi$  and  $\eta\pi$  mass. The  $f_0(980)$  is clearly visible in Fig. 16(g) at 1 GeV. In Figs. 16(h), there is a small but definite  $a_2(1320)$  peak. It does not fit naturally to decays of  $\eta_2(1870)$  and/or  $\eta_2(1645)$ . It is of roughly the right magnitude to originate from  $a_2(1320)\rho$  background. The  $\rho(770)$  signal from this background is also just visible in Fig. 16(g).

On the upper side of the 1850 MeV peak is a small  $2^-$  component, which may be fitted with  $\eta_2(1870)$ . When this contribution is omitted from the fit, log likelihood gets worse by 84. The relative intensities in  $a_0(980)\pi$ ,  $a_2(1320)\pi$ ,  $f_2(1270)\eta$  and  $\sigma\eta$  decays are fixed to accurate values from Crystal Barrel data [31]. Production phases, attached to each amplitude in the isobar model, are fitted freely. So there are five fitted parameters. Statistically, the significance of the  $2^-$  component is 10 standard deviations, despite the signal being small. The reason for this significance is that amplitudes have a distinctive angular dependence which is readily identified. For completeness, a contribution is also included for  $\eta_2(1645)$ . It is much smaller and barely significant. In Ref. [31], it is suggested that  $\eta_2(1645)$  is a standard  $q\bar{q}$  state, the isospin partner to  $\pi_2(1670)$ ;  $\eta_2(1870)$  is interpreted as a hybrid. This interpretation is consistent with the observations here. The production of a hybrid is naturally explained in terms of  $c\bar{c} \rightarrow \gamma gg$ , followed by conversion of one gluon  $g$  to  $q\bar{q}$ .

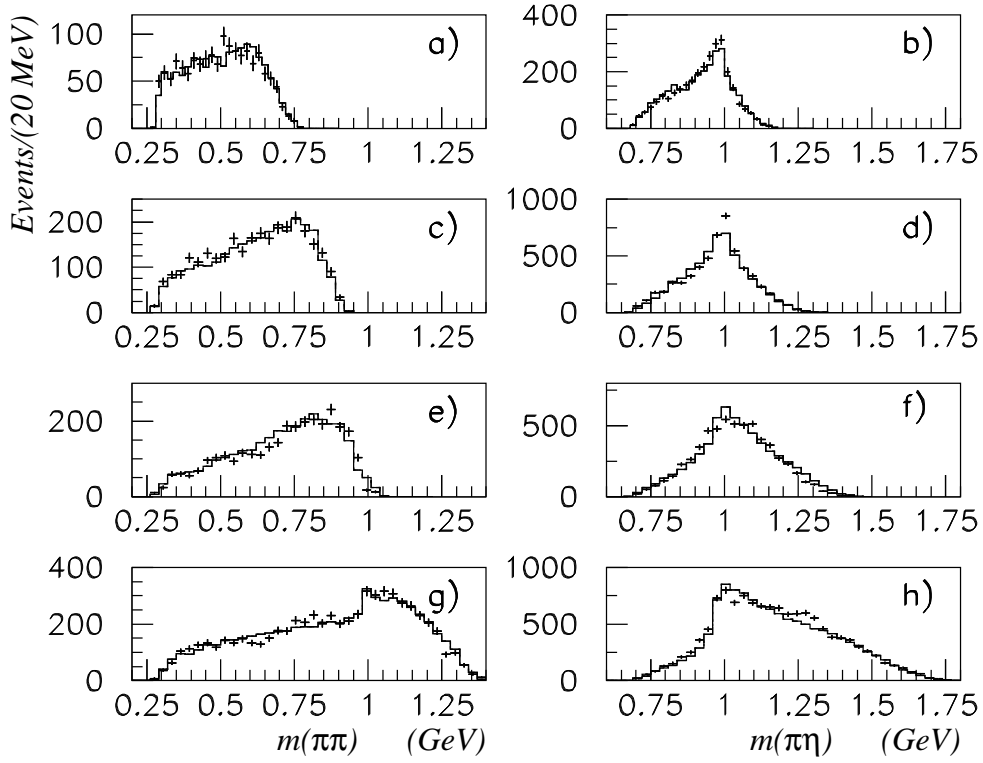


Figure 16: Fits to mass projections on to (a)  $M(\pi\pi)$  and (b)  $M(\pi\eta)$  for the  $\eta\pi\pi$  mass range 1230–1330 MeV, compared with the fit (histogram); (c)–(d) the mass range 1350–1480 MeV; (e)–(f) 1480–1600 MeV; (g)–(h) 1700–1900 MeV.



## 6.1 The magnitude possible for $X(1835) \rightarrow \eta\pi\pi$

The BES Collaboration has presented evidence for an  $X(1835)$  in  $\eta'\pi\pi$  with a production branching fraction  $BR(J/\Psi \rightarrow \gamma X).BR(X \rightarrow \pi^+\pi^-\eta') = [2.2 \pm 0.4(stat) \pm 0.4(syst)] \times 10^{-4}$  and a width of 68 MeV [11]. There is no obvious signal in  $\eta\pi^+\pi^-$  data of Fig. 7, although the fit to data is slightly ragged in this mass range.

A free fit including it with published mass and width gives 189  $f_0(980)\pi$  events, 94  $a_0(980)\pi$ , 164  $\eta\sigma$  and 86  $a_2(1320)\pi$ . Log likelihood improves by 58 for 8 additional fitting parameters. There is flexibility in the fit, and the total number of events can be increased from 533 to 1182 if log likelihood is allowed to get worse by 2 for every channel, corresponding to an overall 4 standard deviation change. This is a cautious limit taking account of the fact that the components fitting this mass range are uncertain. The corresponding branching fraction is  $BR(J/\Psi \rightarrow \gamma X).BR(X \rightarrow \pi^+\pi^-\eta) = 0.38 \times 10^{-4}$ . No statement can be made about its possible coupling to  $K\bar{K}\pi$ , since the mass range of the present data extends only to 1800 MeV.

Huang and Zhu [32] point out that its mass, total width, production rate and decay pattern favour its assignment as the second radial excitation of  $\eta'$ . More precisely, the small branching fraction in  $\eta\pi\pi$  favours a mixing angle between  $n\bar{n}$  and  $s\bar{s}$  close to that of the  $\eta'$ . The  $\eta'(958)$ ,  $\eta(1440)$  and  $X(1835)$  would then form a Regge trajectory with a spacing in  $M^2$  of  $\sim 1.22 \text{ GeV}^2$ , close to that of other well established trajectories [33]. The peak observed by BES2 at 2240 MeV in  $\phi\phi$  would fit naturally as the fourth member of this sequence [34]. However, resonant phase variation needs to be established for  $\eta(1835)$  and the  $\phi\phi$  peak.

Ma [35] tries to interpret  $B(1835)$  as a baryonium state associated with the threshold peak observed in  $\bar{p}p$  in BES data [36]. This interpretation leads to a decay stronger to  $\eta\pi\pi$  than  $\eta'\pi\pi$ , and is clearly ruled out by the present data.

## 7 Interpretation of $\eta(1440)$ and $f_1(1510)$

If there is just one  $\eta(1440)$  in the mass range 1400–1500 MeV, it either has a large SU(3) singlet  $q\bar{q}$  component or a glueball component. Either would explain its strong production in  $J/\Psi$  radiative decays, where  $c\bar{c}$  appear in a singlet combination. It could likewise be produced strongly in  $\bar{p}p$  annihilation. However the  $K^*K$  channel is SU3 octet, so the  $\eta(1440)$  (or  $\eta(1475)$ ) cannot be purely singlet.

It is well known that isolated  $s\bar{s}$  states such as  $f_2(1525)$  are produced weakly in  $\bar{p}p$  annihilation. If the  $\eta(1475)$  is to be produced strongly in  $\bar{p}p$  annihilation, it should have a substantial  $n\bar{n}$  component, but that is inconsistent with decays purely to  $K^*\bar{K}$ . The  $\eta(1405)$  decays much more strongly to  $\kappa K$  and  $f_0(980)\eta$  than to  $\eta\sigma + a_0(980)\pi$ . This would not arise naturally if it is a pure  $n\bar{n}$  state. So the conclusion is that a substantial  $s\bar{s}$  (or glueball) component must be present in  $\eta(1440)$  or  $\eta(1405) + \eta(1475)$ .

The existence of  $\eta(1295)$  depends primarily on data in three papers on  $\pi^-p \rightarrow (\eta\pi\pi)n$  and one on  $\pi^-p \rightarrow (K\bar{K}\pi)n$  [1]. In this process, there should be a clear distinction between  $\eta(1295)$  which decays via the S-wave and  $f_1(1285)$  which decays via the P-wave. If production is limited to a single exchange process, these are immediately distinguishable. In  $\bar{p}p$  annihilation the situation is much more complex, since there are four combinations of  $\eta\pi\pi$  produced in every event [6], making the separation between  $\eta(1295)$  and  $f_1(1285)$  much more difficult. Those

reviews which argue against the existence of  $\eta(1295)$  base their arguments on the fact that there could be more than one exchange mechanism in  $\pi^-p$  production data, leading to possible confusion between the flat angular distribution from  $\eta(1295)$  and rank 2 processes involving  $f_1(1285)$ . It is unfortunate that the papers of primary importance published on  $\eta(1295)$  do not give quantitative estimates of its significance. If the data still survive, it would be valuable if the groups concerned would publish values of log likelihood or  $\chi^2$  showing quantitatively how their fit changes when the  $\eta(1295)$  is omitted. This information would sharpen the arguments for or against  $\eta(1295)$ .

In the data presented here, most of the peak near 1285 MeV certainly is due to  $f_1(1285)$ ; a free fit including  $\eta(1295)$  improves log likelihood only by 3.7 for four parameters fitted to magnitudes and phases of decay amplitudes to  $a_0(980)\pi$  and  $\eta\sigma$ . Seven events are fitted to  $\eta(1295)$  compared with 230 to  $f_1(1285)$ . So the evidence for  $\eta(1295)$  in present data is not significant.

Is the  $\eta(1440)$  really split into two components? Although fit A optimises  $\eta(1405)$  at 1429 MeV, a persistent feature of data fitted to  $\eta(1405)$  in other analyses is a mass 1405 MeV in  $\eta\pi\pi$  and 1414 MeV in  $\kappa\bar{K}$ . As shown in Section 5.3, data from  $\bar{p}p$  annihilation require corrections to these masses for the phase space in the production process. This shifts the mass fitted to  $\eta\pi\pi$  data up by 4.7 MeV and that in  $K\bar{K}\pi$  data by 9.7 MeV. Weighting these with the intensities fitted to  $\eta\pi\pi$  and  $\kappa\bar{K}$  in Table 2, the mean mass of  $\eta(1405)$  becomes 1421 MeV. There is then a discrepancy in mass of  $18 \pm 5$  MeV with the mass in fit A with a single resonance. This is not convincing evidence for two separate resonances near 1440 MeV. However, it must be said that one cannot move the  $\eta(1440)$  much below 1439 MeV without a poor fit to the peak in  $K\bar{K}\pi$ . How could the difference of 18 MeV be explained between  $\eta\pi\pi$  data and  $K\bar{K}\pi$ ?

Klempt [37] has pointed out a possible explanation. A radial excitation has a node in its wave function causing a zero in decays to  $a_0\pi$  in this general mass range. Firstly this attenuates the  $\eta\pi\pi$  signal and may explain why it is weaker than  $\kappa\bar{K}$  and  $K^*\bar{K}$ . Secondly, such a node introduces a further  $s$ -dependence into  $\eta\pi\pi$ . Suppose the amplitude for the  $a_0\pi$  channel is multiplied by a factor  $(s_0 - s)/s_0$ , where  $s_0$  is the location of the zero in the amplitude. A resonance at 1439 MeV can have a peak at 1410 MeV if there is a zero in the amplitude at 1.47 GeV, just where there is a dip in the  $\eta\pi\pi$  mass spectrum, Fig. 7. However, the peak is attenuated more on its upper side than its lower side and the peak is somewhat asymmetric. Tests on the present data show that this explanation does cure the 10 MeV discrepancy between  $\eta\pi\pi$  data and the fit near 1500 MeV. However, a factor 10 higher statistics are needed to test the idea precisely. It cannot be tested in  $\bar{p}p$  annihilation because of the four different charge combinations. Zeros would appear at different masses in  $\eta\sigma$  and  $\kappa\bar{K}$ , depending on matrix elements, leading to a potentially complicated line-shape with peaks at different masses in different channels.

There is one further possible complication. The dominant decay of  $\eta(1440)$  is through  $K\bar{K}\pi$ . There is inevitably some rescattering of  $K\bar{K}$  through  $a_0(980)$  to the  $\eta\pi\pi$  channel via what are called triangle graphs. This was discussed in some detail in Ref. [6]. It will have the effect of increasing the  $K\bar{K}\pi$  decay branching fraction of  $\eta(1440)$ .

Let us turn to  $\eta(1890)$ . The general pattern of the broad components in the  $\eta\pi\pi$  mass projection of Fig. 7 is that there are two components peaking at 1890 and 1600 MeV. It is possible that the latter is resonant. In the  $\gamma 4\pi$  data there is evidence for a resonance at 1970 MeV with a width of 210 MeV. If the parameters of  $\eta(1890)$  are changed to those values, log likelihood for  $\eta\pi\pi$  data is worse by 42. This is a modest amount, in view of the systematic

uncertainties about how to fit the  $\eta\pi\pi$  mass range above 1600 MeV and the strong  $K^*\bar{K}^*$  threshold nearby. It is therefore possible that these two signals arise from the same resonance, though this cannot be proved at the moment.

Consider next  $f_1(1420)$  and  $f_1(1510)$ . In Fig. 8(a), one sees that the effect of  $f_1(1510)$  is to produce a slight bump at 1490 MeV and extend the tail of  $f_1(1420)$ . Longacre [38] has suggested that  $f_1(1420)$  may be an abnormal state (or ‘molecule’ in current terminology) with an  $L = 1$  pion orbiting a  $K\bar{K}$  S-wave combination. In this picture, there are final state interactions from two combinations of  $K^*$  and a further final-state interaction between the two S-wave kaons. My suggestion is that these final state interactions enhance this state strongly at the lowest  $K\bar{K}$  masses, but the rapid rise of the  $K^*\bar{K}$  phase space with momentum produces a long tail extending into the mass region of what is called  $f_1(1510)$ .

It must be said in favour of the data of Aston et al. that they identified the  $h_1(1370)$   $J^{PC} = 1^{-+}$  state and it was subsequently confirmed by Crystal Barrel data [39]. Furthermore, there is a  $2^{-+}$  peak in their data which they did not claim as a resonance, but was subsequently identified as a resonance by Crystal Barrel [40] and confirmed by WA102 [41]. The conclusion is that the data of Aston et al. appear reliable. The primary question is one of interpretation of their  $J^{PC} = 1^{++}$  signal. They did not include  $f_1(1420)$  in their fit. So it is possible that the  $f_1(1420)$  has a more extended line-shape than has previously been fitted.

## 8 Summary

The main experimental results are the observation of three peaks in the  $\eta\pi\pi$  mass spectrum: a narrow peak at 1415 MeV, a shoulder at 1550 MeV and a broad peak at  $\sim 1850$  MeV. In  $K\bar{K}\pi$ , there is an asymmetric peak at  $\sim 1450$  MeV. The asymmetry is due to the  $s$ -dependence of the  $K^*\bar{K}$  channel; its Dalitz plot immediately identifies a dominant  $K^*\bar{K}$  decay. The intensity for that decay increases rapidly from its threshold at  $\sim 1390$  MeV as  $k^3$ , where  $k$  is the momentum of decay  $K$  and  $K^*$  in the  $K^*K$  rest frame.

An essential point from the present analysis is that one must include this  $s$ -dependence correctly into the Breit-Wigner amplitude. This reduces the mass of  $\eta(1475)$  to 1440 MeV.

When analysing  $\bar{p}p$  data, it is necessary to allow for the variation of phase space for production of  $\eta\pi\pi$  and  $\kappa\bar{K}$  with mass. This corrects the mass of  $\eta(1405)$  upwards by 4.7 MeV in  $\eta\pi\pi$  and by 9.7 MeV in  $\kappa\bar{K}$ . As a result, the mean mass difference between the possible  $\eta(1405)$  and  $\eta(1440)$  is no larger than  $18 \pm 5$  MeV.

There is a dominant broad  $0^-$  amplitude in  $\eta\pi\pi$ . When this is included into the partial wave fit, interference with a single  $\eta(1440)$  can account naturally for the observed peaks at 1415 MeV in  $\eta\pi\pi$  and at 1450 MeV in  $K\bar{K}\pi$ . There is no evidence for two separate  $\eta(1405)$  and  $\eta(1475)$  from the present data.

The  $\eta(1835)$  is not observed in the present  $\eta\pi\pi$  data, and an upper limit has been derived for the branching fraction for its production in  $J/\Psi$  decays. This limit is a factor  $5.7 \pm 1(stat) \pm 1(syst)$  smaller than the  $\eta(1835)$  observed in the  $\eta'\pi\pi$  channel. The natural explanation is that  $\eta(1835)$  is a radial excitation of  $\eta'$  and  $\eta(1440)$ .

As an aid to further work, the fully annotated Fortran code for the broad  $0^-$  component and  $\eta(1440)$  is available from the author. This code includes numerical values of  $g^2$  from the present work, but they would need to be re-optimised if further data become available.

I wish to acknowledge financial support from the Royal Society and major help from members of the BES collaboration in processing data and running the Monte Carlo simulation of acceptance and backgrounds.

## References

- [1] Particle Data Group (PDG), Physics Letters **B667** 1 (2008)
- [2] S. Fukui *et al.*, Phys. Lett. B **267** 293 (1991)
- [3] D. Alde *et al.* (GAMS Collaboration), Yad. Fis. **60** 458 (1997), translated in Part. At. Nuclei **60** 386 (1997)
- [4] J.J. Manak *et al.* (E852 Collaboration), Phys. Rev. **D62** 012003 (2000)
- [5] G.S. Adams *et al.* (E852 Collaboration), Phys. Lett. **B516** 264 (2001)
- [6] A.V. Anisovich *et al.*, Nucl. Phys. A **690** 567 (2001)
- [7] E. Klempt and A. Zaitsev, Phys. Rep. **454** 1 (2007)
- [8] A. Masoni, C. Cicalo and G.L. Usai, J. Phys. G: Nucl. Phys. **32** R293 (2006)
- [9] C.J. Morningstar and M. Peardon, Phys. Rev. **D60** 034509 (1999)
- [10] R. Escribano, arXiv: hep-ph/0802.3909
- [11] M. Ablikim *et al.* (BES Collaboration), Phys. Rev. Lett. **95** 262001 (2005)
- [12] J.Z. Bai *et al.* (BES Collaboration), Nucl. Instr. Methods **A344** 319 (1994)
- [13] J.Z. Bai *et al.* (BES Collaboration), Nucl. Instr. Methods **A458** 627 (2001)
- [14] D. Edwards *et al.* (Crystal Ball Collaboration), Phys. Rev. Lett. **51** 859 (1983)
- [15] D.V. Bugg, accompanying paper arXiv:0907.3021
- [16] Z. Bai *et al.* (Mark III Collaboration), Phys. Rev. Lett. **65** 2507 (1990)
- [17] M. Ablikim *et al.* (BES Collaboration), Phys. Lett. B **598** 149 (2004)
- [18] M. Ablikim *et al.* (BES Collaboration), Phys. Lett. **B633** 681 (2006)
- [19] D.V. Bugg, Phys. Lett. B **632** **471** (2006)
- [20] D. Aston *et al.* (LASS Collaboration), Nucl. Phys. B **296** 493 (1988)
- [21] B.S. Zou and D.V. Bugg, Phys. Rev. **D48** R3948 (1993)
- [22] D.V. Bugg, J. Phys. **G34** 151 (2007)

- [23] B.S. Zou and D.V. Bugg, Eur. Phys. J **A 16** 537 (2003)
- [24] D.V. Bugg, Phys. Rev. D **78** 074023 (2008)
- [25] D.V. Bugg, A. V. Sarantsev and B.S. Zou, Nucl. Phys. B **471** 59 (1996)
- [26] M. Ablikim *et al.* (BES Collaboration) Phys. Lett. **B607** 243 (2005)
- [27] D. Aston *et al.* (LASS Collaboration) Phys. Lett. **B201** 573 (1988)
- [28] A.V. Anisovich *et al.* Phys. Lett. **B472** 168 (2000)
- [29] P. Baillon *et al.*, Nu. Cim. **50A** 383 (1967)
- [30] C. Amsler *et al.* (Crystal Barrel Collaboration), Phys. Lett. **B358** 389 (1995)
- [31] A.V. Anisovich *et al.* (Crystal Barrel Collaboration), Phys. Lett. B **477** 19 (2000)
- [32] T. Huang and S-L. Zhu, Phys. Rev. **D73** 014023 (2006)
- [33] D. V. Bugg, Phys. Rep. **297** 257 (2004)
- [34] M. Ablikim *et al.*, (BES Collaboration), Phys. Lett. **B662** 330 (2008)
- [35] Y-L. Ma, arXiv: 0803.3764
- [36] M. Ablikim *et al.* (BES Collaboration), Phys. Rev. Lett. **95** 262001 (2005)
- [37] E. Klempt, hep-ph/0409148 and Beijing 2004, ICHEP 2004, vol. 2, p1082
- [38] R.S. Longacre, Phys. Rev. **D42** 874 (1990)
- [39] A. Abele *et al.* (Crystal Barrel Collaboration), Phys. Lett. **B415** 280 (1997)
- [40] J. Adomeit *et al.* (Crystal Barrel Collaboration), Z. Phys. C **71** 227 (1996)
- [41] D. Barberis *et al.* (WA102 Collaboration), Phys. Lett. **B413** 217 (1997)